3rd International Symposium on Integrating CFD and Experiments in Aerodynamics
20-21 June 2007
U.S. Air Force Academy, CO, USA

An Experimental and Computational Investigation of a 3D, l/h=5 Transonic Cavity Flow

K. Knowles
S. A. Ritchie
Department of Aerospace, Power and Sensors
Cranfield University
Defence Academy of the UK
Shrivenham, SN6 8LA. UK
k.knowles@cranfield.ac.uk

N. J. Lawson
Dept of Aerospace Sciences
School of Engineering
Cranfield University
Bedfordshire, MK43 0AL, UK

Abstract

This paper presents an investigation of a transonic flow (M = 0.85) over a rectangular cavity having a length-to-depth ratio of 5. Velocities were measured inside the cavity on the central plane and two off-centre planes using a two-component particle image velocimetry system. These measurements were supported by surface flow visualisation, and mean and time-varying surface pressure measurements. The flow was also simulated using an unsteady Reynolds-averaged Navier Stokes code, with a realizable k-ε turbulence model. It is shown that this CFD model does not capture all the characteristics of the flowfield correctly. However, by using this integrated experimental and computational approach we have been able to identify the presence of new vortical structures within the cavity and point out the importance of free shear layer flexibility in the cavity oscillation process.

Key words: transonic, aerodynamics, cavity flows, stores release, PIV, URANS, realizable k-ε turbulence model

Introduction

The phenomenon of flow within a rectangular cavity immersed in transonic flow has become the focus of much research interest recently due to the importance of stealth (and aerodynamic efficiency) in future manned aircraft such as the F-35 Lightning II, and various unmanned combat air vehicle (UCAV) projects. These aircraft are designed such that the internal carriage of weapons is vital in maintaining a low radar cross-section, which in turn increases the vehicle's survivability. However, when the weapons bay doors are opened for weapons release, flow over the exposed cavity causes a number of undesirable effects. These include self-sustaining acoustic oscillations and high intensity tones which can lead to structural fatigue in 'open' cavity flows [1] (occurring, primarily, in cavities with low length-to-depth ratios, l/h) and adverse longitudinal pressure distributions leading to nose-in pitching moments on stores released in 'closed' cavity flows [2] (primarily for high l/h).

Many previous studies on cavity flows have been either solely experimental, usually involving surface pressure measurements, or computational with validation against existing experiments. Much of the early research on cavity flows concentrated on empty cavities, although there are now a few studies with representative stores in a cavity. Recently, the rapid development of advanced optical measurement techniques such as particle image velocimetry (PIV) [3] and laser Doppler anemometry (LDA) [4] has allowed detailed quantitative flow velocity data to be acquired with no physical intrusion into the flow. There are only limited velocity data available in the literature for transonic cavity flows and these are confined to the centre-line of an empty cavity [5].

Report Documentation Page

Form Approved
OMB No. 0704-0188

1. REPORT DATE	2. REPORT TYPE	3. DATES COVERED
JUN 2007	**N/A**	**-**

4. TITLE AND SUBTITLE	5a. CONTRACT NUMBER
An Experimental and Computational Investigation of a 3D, l/h=5 Transonic Cavity Flow	5b. GRANT NUMBER
	5c. PROGRAM ELEMENT NUMBER
6. AUTHOR(S)	5d. PROJECT NUMBER
	5e. TASK NUMBER
	5f. WORK UNIT NUMBER
7. PERFORMING ORGANIZATION NAME(S) AND ADDRESS(ES) **Department of Aerospace, Power and Sensors Defence Academy of the UK Cranfield University Shrivenham, SN6 8LA. UK**	8. PERFORMING ORGANIZATION REPORT NUMBER
9. SPONSORING/MONITORING AGENCY NAME(S) AND ADDRESS(ES)	10. SPONSOR/MONITOR'S ACRONYM(S)
	11. SPONSOR/MONITOR'S REPORT NUMBER(S)

12. DISTRIBUTION/AVAILABILITY STATEMENT
Approved for public release, distribution unlimited

13. SUPPLEMENTARY NOTES
Third International Symposium on Integrating CFD and Experiments in Aerodynamics, June 2007, The original document contains color images.

14. ABSTRACT

15. SUBJECT TERMS

16. SECURITY CLASSIFICATION OF:			17. LIMITATION OF ABSTRACT	18. NUMBER OF PAGES	19a. NAME OF RESPONSIBLE PERSON
a. REPORT	b. ABSTRACT	c. THIS PAGE			
unclassified	**unclassified**	**unclassified**	**UU**	**47**	

In this paper, the application of PIV, surface pressure measurements, surface flow visualisation and CFD to transonic cavity flows is presented. Data are acquired from a rectangular cavity of length-to-depth ratio l/h=5 at a freestream Mach number of 0.85 using a commercially-available digital PIV system and window deformation processing software. Time-averaged, two-dimensional PIV results are presented for a number of streamwise planes taken from across the width of the cavity. Further data were obtained using time-averaged URANS (unsteady, Reynolds-averaged Navier-Stokes) CFD predictions. The current research programme has included similar investigations on other geometries (l/h = 10, 14) and has included the effect of the presence of representative stores (1, 2 or 3) in the exit plane. Discussion of these cases is beyond the scope of the present paper, which focuses on the integration of the various techniques used to produce an understanding of this complex, three-dimensional flowfield.

Experimentation

All cavity measurements were conducted using the Cranfield University Shrivenham transonic wind tunnel. This is a closed circuit, ejector-driven tunnel with a working section of 206mm (height) by 229mm (width) and a run time of about 10 seconds at M_∞=0.85. The flow in the cavity is described with reference to an orthogonal axis system (x, y, z) aligned with the principal axes of the cavity (see Figure 1). The corresponding flow velocity components u, v and w are also aligned with the principal axes.

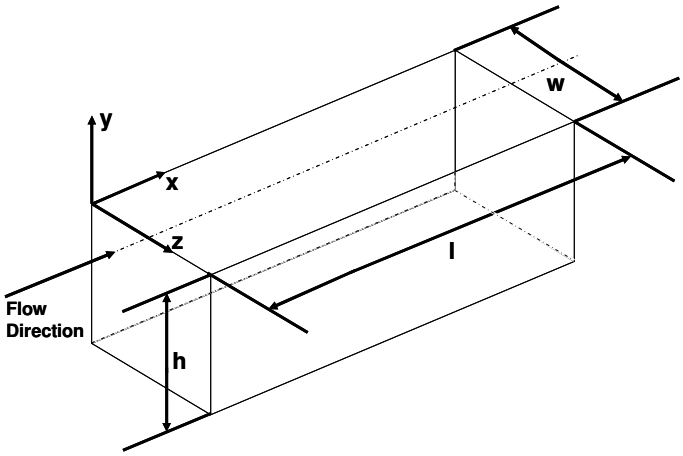

Figure 1. Cavity Geometry and Axis System

The PIV measurements were performed using an optically-transparent cavity mounted in a modified tunnel sidewall. The clear cavity was constructed from polycarbonate and was attached to the underside of a raised flat plate which also acted as a splitter for the tunnel wall boundary layer. An in-house flow seeding system provided around 10μm diameter water seeding. The seeding was injected through a rake of three water atomiser nozzles, equi-spaced across the wind tunnel contraction section and supplied at 140 bar.

The PIV acquisition system consisted of a Dantec FlowMap 500 processor, a Kodak ES1.0 CCD camera and a New Wave Gemini Nd:YAG pulsed laser. The Kodak ES1.0 camera frame rate and laser repetition rate allowed data to be recorded at up to 15Hz. This frame rate was too low to capture the unsteady phenomena in the cavity. Therefore time-averaged flow data derived from the instantaneous data are presented from the PIV. The light sheet was projected into the cavity through the clear floor. The seeded light sheet was viewed perpendicularly via a surface-coated mirror angled at 45° to the cavity right side wall (see Figure 2). PIV data were taken for the same three planes across the cavity on which pressure data were acquired (see below).

To process the PIV images, DaVis software by La Vision was used. The software employs an iterative image-deformation algorithm, similar to those reviewed by Scarano [6], which more effectively extracts vectors from complex rotating flows with high velocity gradients (as seen in deep cavities). The window deformation technique deforms the interrogation region in the second frame according to the velocity gradient present within that region. This leads to identical displacements for all the seeding particles within a region giving an improved signal-to-noise ratio and thus higher accuracy. To process the images, 4 passes were used with two passes at 32x32 and two passes at 16x16. All regions were 75% overlapped in x and y. To aid clarity, the presented vector maps were post-processed by sub-sampling by a factor of 3. Based on the seeding response, the geometry error and the processing error, estimated accuracy in this case is better than 3.4% of full scale measurement.

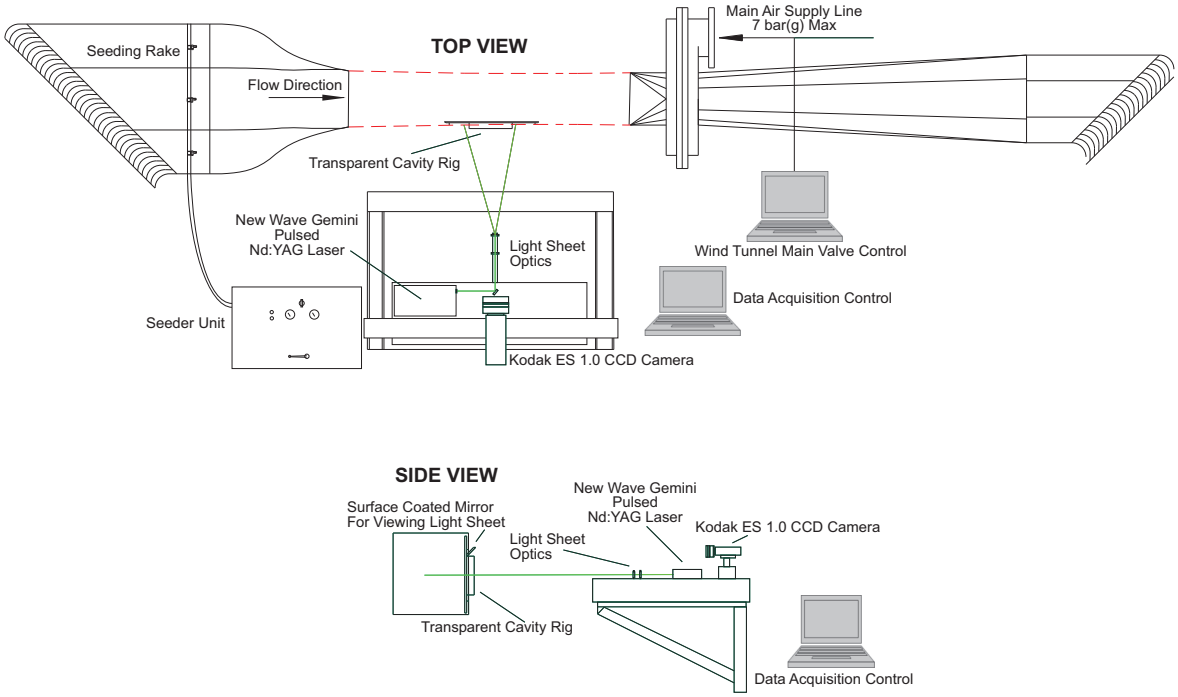

Figure 2. PIV Experimental Set-up

Cavity wall pressures were measured using a modified model of metal construction with three rows of 9 pressure tappings each on the floor of the cavity at z/w = 0.5, 0.667 and 0.833 (referred to as the CL, OC1 and OC2 planes respectively). These tappings were connected via short lengths of tubing to a Scanivalve ZOC block – an electronically-scanned pressure transducer with 32 piezo-resistive pressure sensors. The accuracy of this system is determined to be better than 0.5%, with a 95% confidence level.

The surface flow visualisations were performed using a paraffin-based solution containing solar yellow fluorescent paint particles. By subjecting the particles to ultraviolet (UV) light, the surface flow patterns were clearly visible and could be photographed using digital still photography.

Computation

The three-dimensional numerical simulation presented here was performed using 952000 quadrilateral cells in a half-domain construction with a plane of symmetry used to reduce the computational resource requirements. This was deemed acceptable since the flow within open geometry cavities has been described as largely symmetrical

about the centreline plane in a number of previous studies [7]. A URANS approach using the realizable k-ε turbulence model was employed. This turbulence model was chosen as it includes modifications over the standard k-ε model which make it more suitable for use in flows containing regions of high shear and swirl [8]. The domain construction for the numerical simulation can be seen in Figure 3. The simulation was performed using time steps of 1.76×10^{-5} seconds and was run until all the start-up transients were purged from the solution and the flow had reached a steady state oscillation. Once steady state was attained, the solution was run for a further 20000 time steps in order to allow unsteady pressure data to be collected from the simulation.

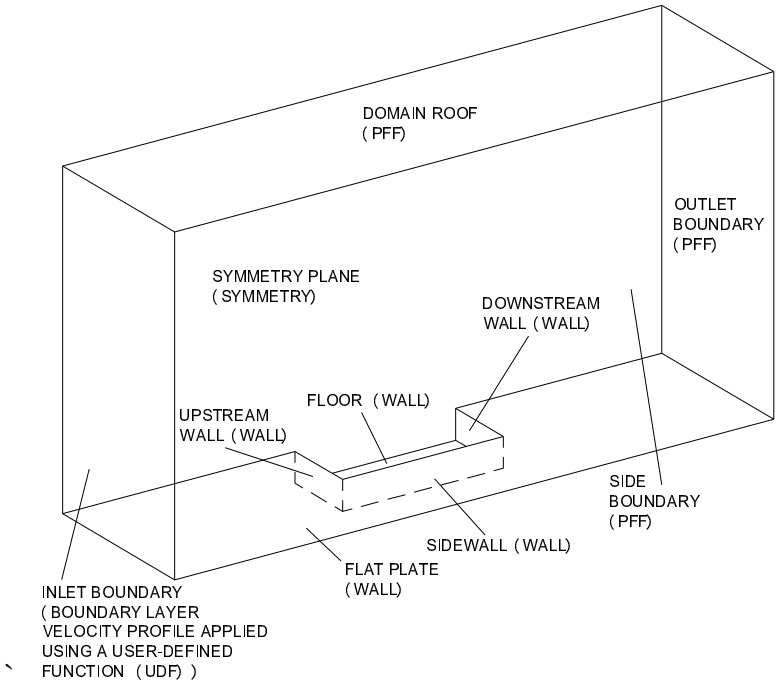

Figure 3. Three-dimensional CFD Domain Construction and Boundary Types

Results

Time-averaged Pressure Data

The experimental and numerical time-averaged pressure coefficient data are shown for the three planes within the cavity in Figure 4. The three experimental spanwise distributions show close agreement in trend along the entire cavity length. On the OC2 plane, the Cp values over the first 60% of the cavity length are lower than the CL and OC1 planes' values suggesting an increased level of flow separation closer to the sidewalls of the cavity. In the downstream 40% of the cavity, the spanwise positions show similar trends, however, there are slight variations in the peak Cp values. The Cp along the first 60% of the cavity floor shows a slight decrease moving downstream which reaches a minimum at approximately x/l = 0.4 where the Cp values are negative. There is a rapid increase in Cp over the downstream 40% of the cavity length reaching a maximum recorded value at x/l = 0.9. The pressure distributions within the cavity are typical of flow on the boundary between open-type and transitional-open-type flow behaviours.

The numerical simulation pressure distributions show a variation from the trend measured experimentally over the streamwise range of experimental measurement (x/l = 0.1-0.9). The profiles show a trend which varies from marginally negative to marginally positive along the first 85% of the cavity length before a C_p rise to peak values

caused by flow stagnation at the downstream wall. The trend and C_p values of the numerical profiles across the three planes show close agreement, which is consistent with the observations made in the experimentally-measured profiles. The highest peak C_p within the cavity is seen on the CL plane with the OC1 and OC2 planes showing the second and third highest peak values respectively. This is also consistent with the observations from the experimental data. At the final streamwise tapping in the experimental data (x/l = 0.9), the experimental C_p values on the CL and OC1 planes are higher than the corresponding numerical values, which can be attributed to a difference in the flow type being exhibited within the cavities. The C_p profiles for the numerical simulation are typical of those seen in a cavity exhibiting open-type flow behaviour compared with the open/transitional-open flow behaviour seen experimentally.

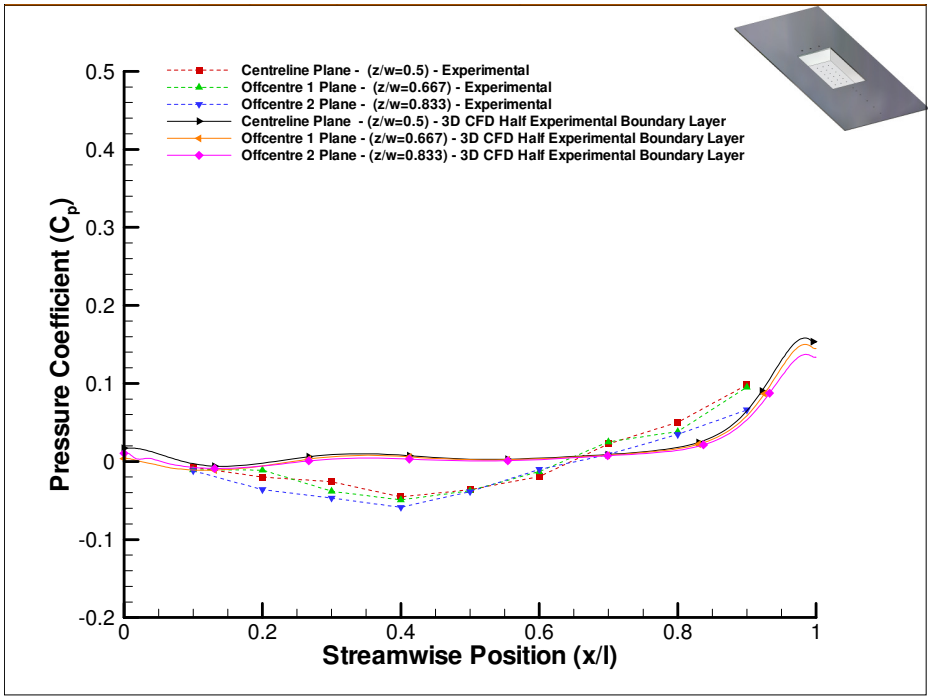

Figure 4. Comparison of Mean Pressure Coefficient Profiles: Experiment vs 3D CFD, Half-Domain Simulation

Unsteady Pressure Data

Figure 5 shows the unsteady pressure spectra for the x/l=0.9 pressure tapping on the CL plane for the experimental and numerical cases. Both spectra show the presence of high intensity peaks within the signal, the frequencies of which are compared with the theoretical Rossiter frequencies calculated using the 'modified-Rossiter' equation [9] in Table 1 along with the corresponding frequencies for the OC1 and OC2 planes.

The correlation between the theoretical and experimental oscillation characteristics is excellent for the 1st and 3rd Rossiter modes with the experimental data showing less than 0.5% variation from the theoretical data in both modes. The numerical simulation shows a slightly larger mode frequency variation of 9.5% from the theoretical value for the 1st mode and 3.8% from the theoretical from the 3rd mode. The 2nd mode data show a 2.4% variation on the CL plane rising to a 5.3% variation on the OC2 plane compared with the theoretical values. The 2nd mode peaks in the numerical simulation spectra are not visible above the background noise level suggesting attenuation of the 2nd mode oscillation in the simulation. The cavity is shown to be oscillating with a 1st mode dominance in both the experimental and numerical cases which suggests that the simulation has successfully predicted the oscillation

feedback mechanism within the cavity. The experimental 1st mode peak SPL of 161dB compares favourably with the 155dB 1st mode peak seen in the numerical solution. The highest discernable oscillation mode in both the experimental and numerical data is the 3rd mode, after which the background noise level swamps any frequency peaks.

Table 1. Comparison of l/h=5 Theoretical, Experimental and Numerical Rossiter Mode Frequencies

Rossiter Mode Number	*Theoretical Oscillation Frequency (Hz)*	*Experimental Oscillation Frequency (Hz*	*Numerical Oscillation Frequency (Hz)*
1	461.88	CL - 463.65	CL – 510.54
2	1131.29	CL – 1074.97	CL – No Peak
3	1800.70	CL – 1795.93	CL – 1873.56
1	461.88	OC1 -463.65	OC1 – 510.54
2	1131.29	OC1 – 1084.94	OC1 – No Peak
3	1800.70	OC1 – 1795.94	OC1 – 1873.56
1	461.88	OC2 -463.65	OC2 – 510.54
2	1131.29	OC2 – 1104.51	OC2 – No Peak
3	1800.70	OC2 – 1792.96	OC2 – 1869.71

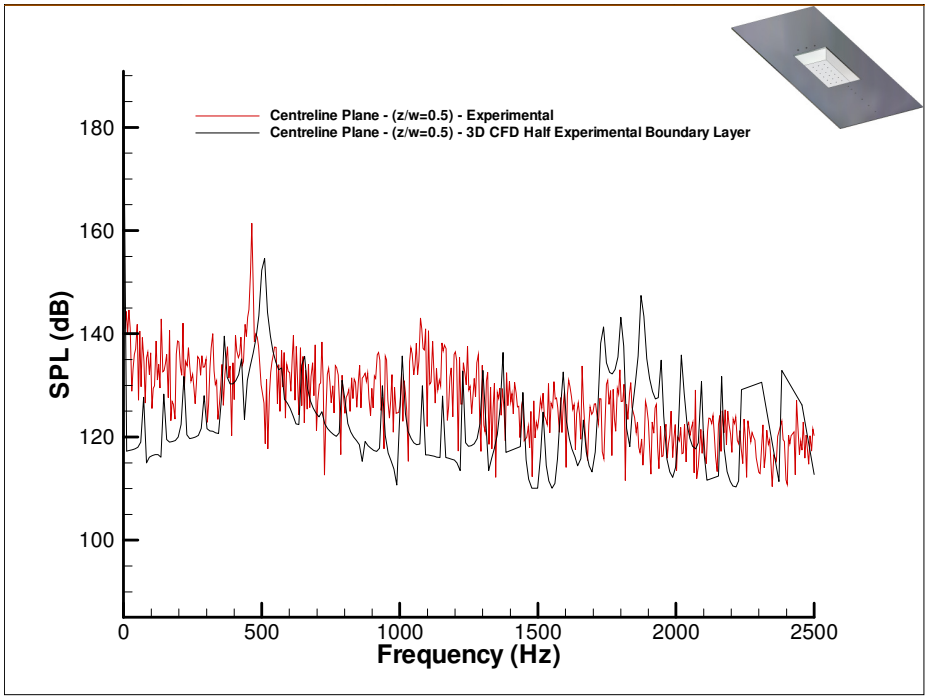

Figure 5. Comparison of Unsteady Pressure Spectra at x/l=0.9: Experimental vs 3D CFD, Half-Domain Simulation – Centreline Plane

Surface Flow Visualisation

The pressure coefficient profiles and unsteady spectra have been used to identify the type of flow and oscillation modes occurring within the cavity; a more detailed description of the flow behaviour and structure, however, is not

possible from these data alone. Description of the flow behaviour can be further developed with reference to the surface flow visualisation study.

A graphical representation of the experimental surface oil-flow pattern photograph can be seen in Figure 6 and shows the surface streamlines on the cavity floor, sidewalls, upstream and downstream walls. The graphic representations are based on a topology defined by Hunt *et al*. [10] during oil flow studies of flow around obstacles on a flat plate. The numerical simulation equivalent of these surface streamlines can be seen in Figure 7.

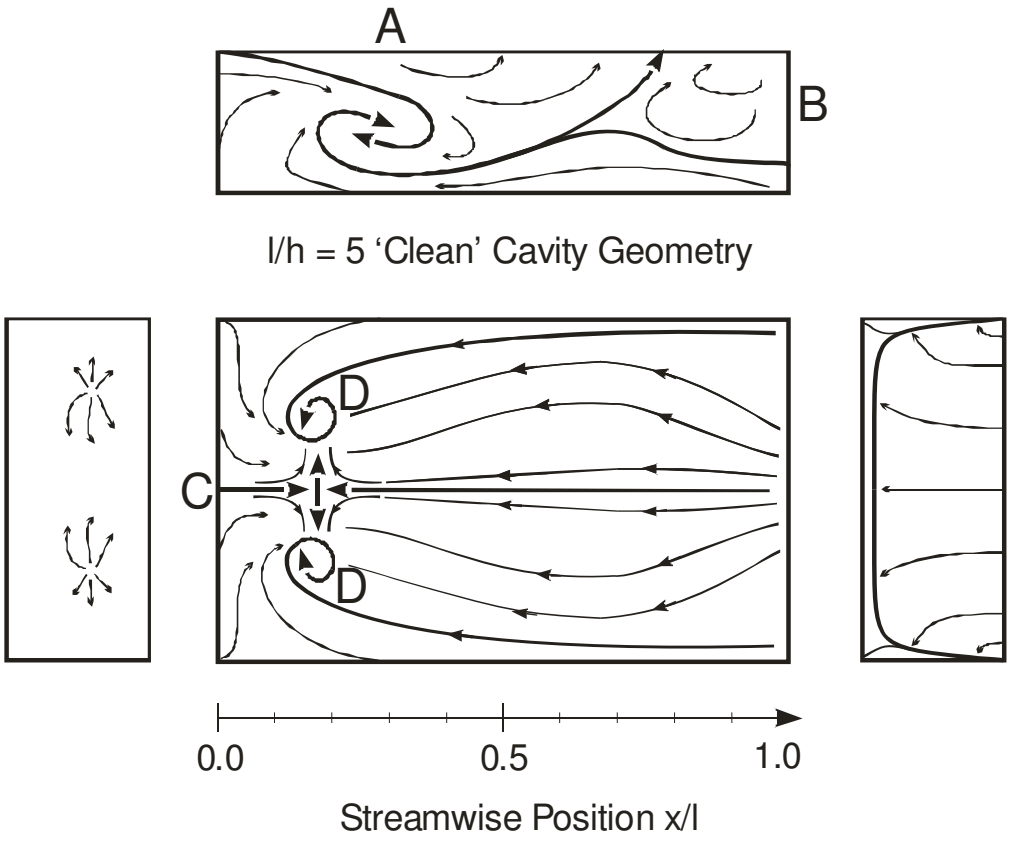

Figure 6. Graphical Representation of Oil Flow Visualisations

In both the experimental and numerical cases, the streamlines on the floor of the cavity show that the flow is travelling against the freestream direction over most of the length which, initially, is consistent with a large single recirculation region in the cavity rotating clockwise for a freestream flow travelling left to right. However, closer inspection reveals that the experimental streamlines show evidence of a recirculation region in the downstream end of the cavity. Both the recirculations rotate with the same sense and "with" the freestream flow. This twin recirculation flow structure is supported by the streamlines on the cavity sidewalls. In the numerical solution, there is no evidence of a smaller secondary recirculation and the main recirculation (A) reaches the downstream wall of the cavity. The difference in surface streamlines between the experimental and numerical cases suggests that the shear layer deflection into the cavity is much reduced in the numerical simulation resulting in the shear layer passing over the cavity without being subjected to the flow deflections seen in the experimental data that result in the twin-recirculation structure.

In both cases, the cavity floor streamlines show two contra-rotating flow structures ('D') either side of the centreline plane which show flow rotation in towards the centreline of the cavity much like a focus sink. The structures are 'tornado-like' vortices which spiral up towards the mouth plane of the cavity and, based upon structures seen in the

side wall streamlines in both cases, meet the shear layer at approximately 10% of the cavity depth (y/h = -0.1) where they are entrained into the streamwise flow. The structures are formed when the flow travelling upstream along the floor of the cavity reaches the natural flow boundary formed by the upstream wall. The proximity of the cavity sidewall forces the flow to divert in the spanwise direction towards the centreline of the cavity. When the flow reaches the CL plane, it meets the flow from the other side of the centreline and is forced to turn to flow downstream but is prevented from doing so by the flow travelling upstream along the cavity floor. The flow is forced to turn out towards the sidewall of the cavity which forms the vertical 'tornado-like' structure seen on the cavity floor.

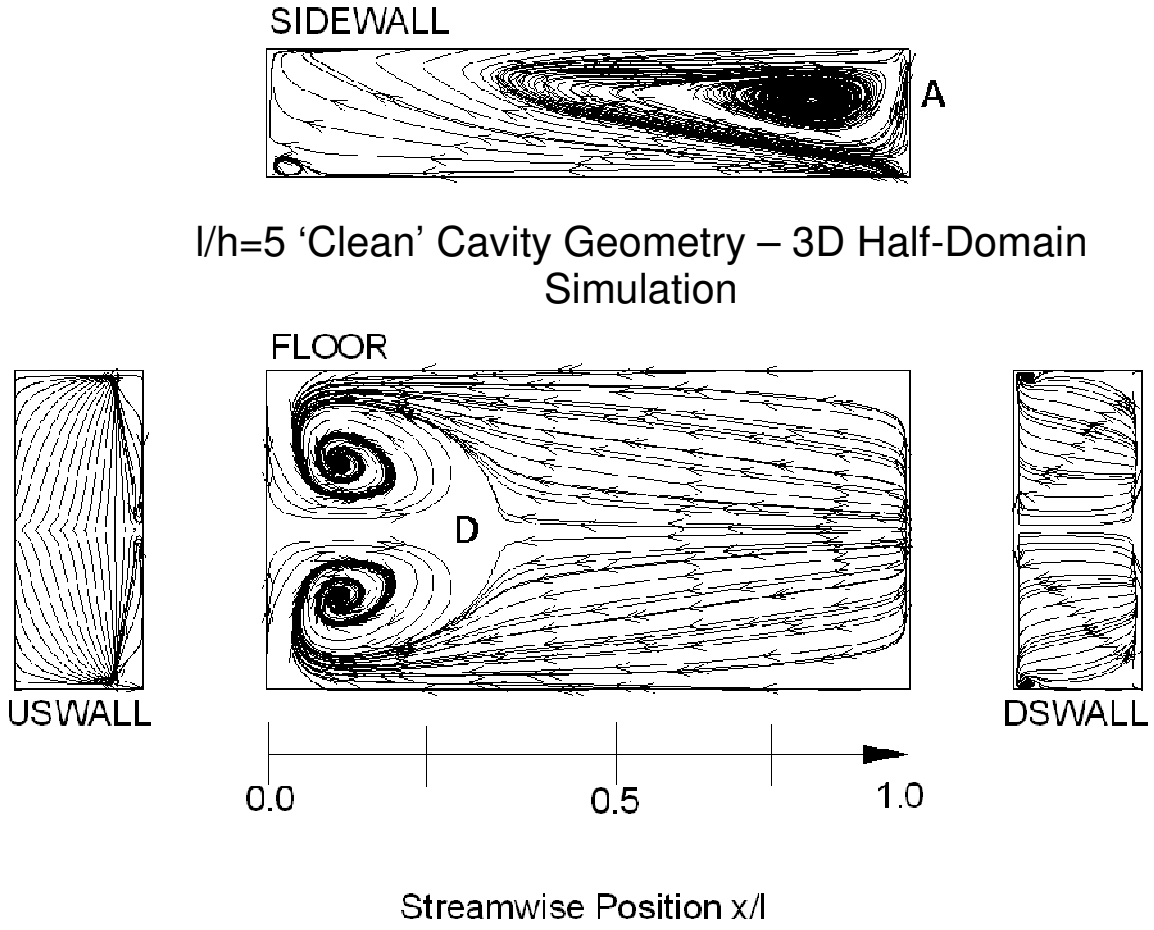

Figure 7. Surface Streamlines from 3D CFD, Half-Domain Simulation

Figure 8 shows stream traces of the flow within the cavity for the numerical simulation. The traces clearly show the existence of the vertical flow structures ('D') in the upstream end of the cavity which were predicted based on the surface flow visualisations. The experimental techniques used during this study could not have visualised these structures in the same way as is possible in the numerical simulation due to the 2D nature of the PIV measurements performed which only provide in-plane velocity data. The ability to derive such extra detail from a validated numerical simulation is vital in better understanding the complexities of flow structures.

Overall, the surface flow visualisations suggest (as with the pressure data) that the flow behaviour within the cavity is open/transitional-open in the experimental study and open in the numerical study. The difference is due to the reduction in shear layer deflection into the cavity seen at the downstream wall of the simulation compared with experimental data. The boundary layer thicknesses are the same in both cases, which suggests that the numerical simulation of the boundary layer results in a shear layer over the cavity which does not have the same level of flexibility as the experimental shear layer. The stiffer shear layer appears to retain its streamwise path over a longer distance and hence does not show a deflected path at the downstream wall.

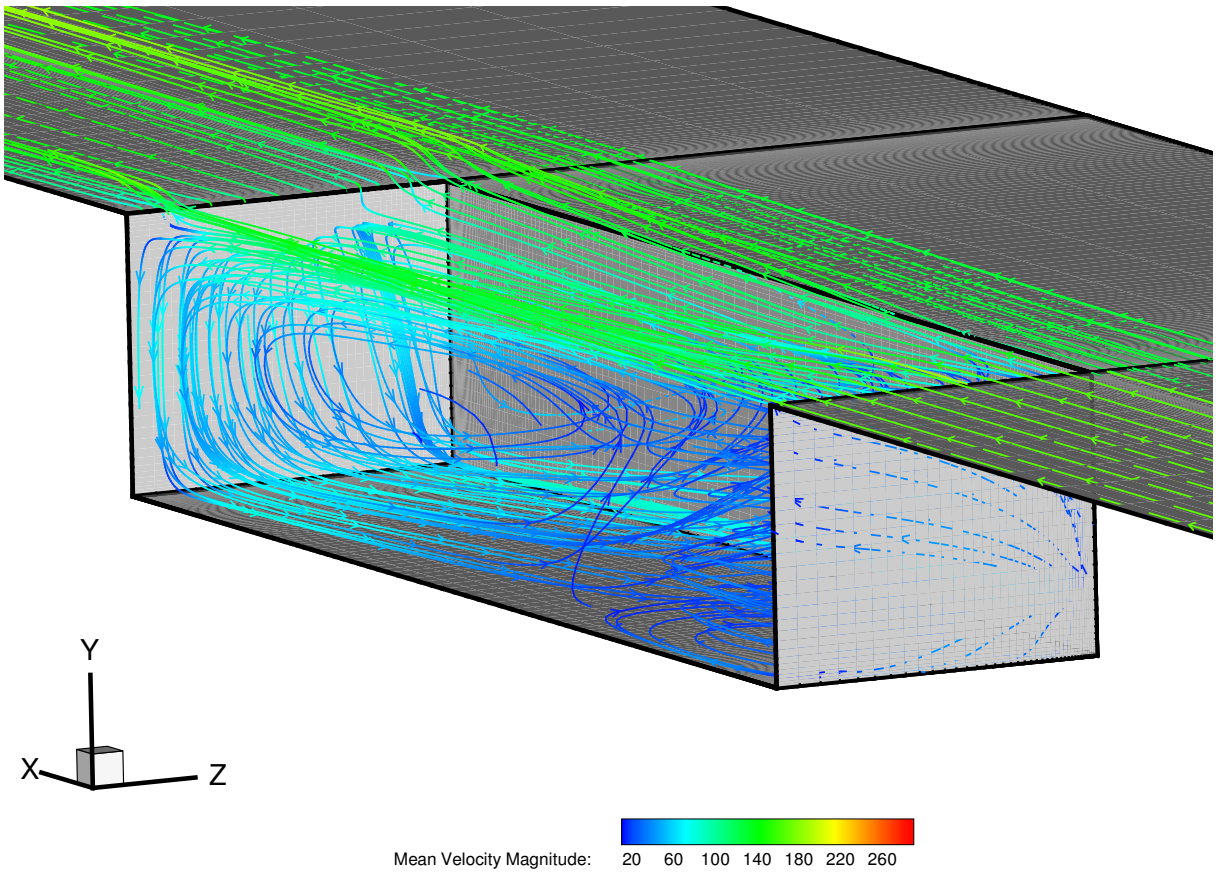

Figure 8. Streamlines of Flow in and Around the Cavity Coloured by Velocity Magnitude: 3D, Half Domain Simulation (for clarity the cavity is not mirrored about the centreline plane)

Flowfield Data

A set of 700 image pairs were acquired with the PIV system per run at a 15Hz sampling rate and processed into instantaneous then time-averaged vector maps using the window-deformation FFT code. The vector data presented are under-sampled 3 times in order to aid the clarity of the flow structures. Figure 9 shows the vector map flow field data for the three planes within the experimental cavity.

The numerical simulation data is presented in the same format as the experimental PIV data in order to allow direct comparison. As described above, the time-averaged flow fields for the numerical solution are generated as the average of 20000 time steps. Figure 10 shows the flow field vector maps for the three planes within the numerical simulation.

On the CL plane, the experimental flow structure extracted contains a large recirculation which is centred at x/l=0.5, y/h=-0.5 and a second smaller recirculation centred at x/l=0.75, y/h=-0.87 which is consistent with the surface flow visualisations. The processing algorithm is unable to extract fully the details of the two flow features at the junction between the two recirculations as the flow directions are directly opposed which leads to difficulty in estimating the particle shift between the first and second frames in the pair. As a result, the upstream extents of small recirculation and the downstream extents of large recirculation are not well defined. The peak velocity magnitude in the centreline plane is approximately V=140ms^{-1} (52% of freestream value) which is seen in the deflected shear layer

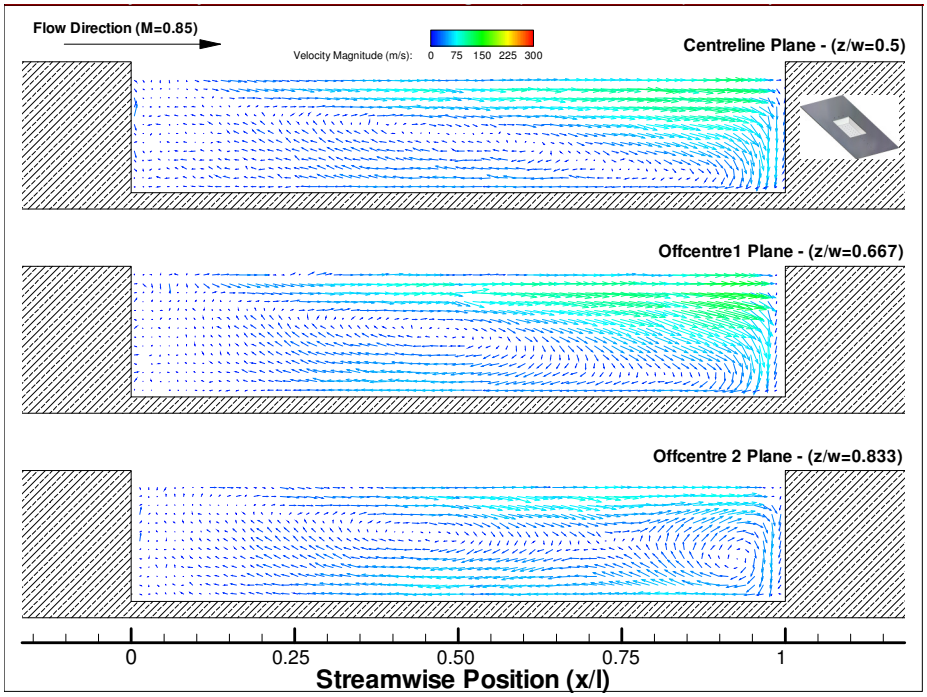

Figure 9. Time-averaged Velocity Vector Maps (window-deformation algorithm)

near the downstream wall. The peak vertical velocity in the CL plane is v=80ms^{-1} and occurs directly adjacent to the downstream wall. This compares well with the numerical simulation data which shows a single large recirculation within the cavity. The peak velocity in the CL plane in the area of the flow visible during the experimental PIV study is V = 113ms^{-1} (41.85% freestream value) and is seen in the maximum shear layer deflection at x/l = 0.85. This peak velocity is 23ms^{-1} lower than the peak value measured experimentally, however, the variation can be attributed to the difference in the shear layer deflections in the two cases. In the experimental study, the shear layer was seen to have a deep deflection into the cavity at the downstream wall. This causes an acceleration of the flow over the deflected shear layer into the cavity near the downstream wall, which is where the V = 140ms^{-1} peak velocity was measured. Although the simulation has the same boundary layer thickness as the experimental study, it is thought that the simulation results in a shear layer which does not show the same growth rate as that seen experimentally. The peak vertical velocity within the cavity is v = 77ms^{-1}, which shows excellent agreement with the peak vertical velocity measured in the PIV study. In both cases, the peak velocity is seen directly adjacent to the downstream wall where the internal flow is forced to recirculate within the cavity.

The OC1 mean flow field shows close similarity in terms of flow structure to the centreline plane in the experimental and numerical cases which is consistent with the flow behaviour predicted from the surface pressure

and streamline studies. Experimentally, the large recirculation ('A') is centred at x/l = 0.5, y/h = -0.5 and the second recirculation ('B') centred at x/l = 0.75, y/h = -0.87 whilst the single recirulcation in the numerical case is centred at x/l = 0.79, y/h = -0.51. The peak experimental velocity magnitude in the plane is approximately V = 140ms^{-1} (52% of freestream value) which, as for the CL plane, occurs in the deflected shear layer. The peak vertical velocity is also very similar to the CL plane value at v = 80ms^{-1}. The peak numerical velocity in the area of the flow visible in the PIV study is V = 113ms^{-1} in the small region of the shear layer which is deflected in to the cavity at x/l = 0.84. This is in excellent agreement with the data from the CL plane. The peak value is 27ms^{-1} lower than the values measured in the experimental study for the same reasons as described above. The peak vertical velocity in the OC1 plane is v = 76ms^{-1}, and shows good agreement with the v = 80ms^{-1} peak vertical velocity measured at the same place in the PIV data.

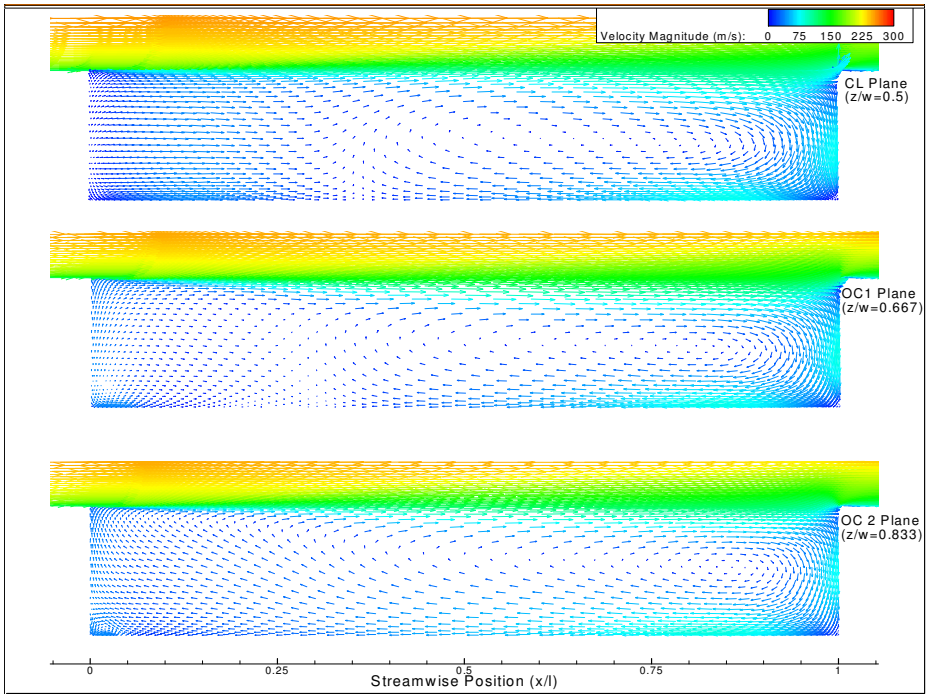

Figure 10. Time-averaged Velocity Vector Maps (3D, half-domain simulation)

The experimental OC2 plane shows a very different flow structure to those measured in the CL and OC1 planes. The downstream recirculation ('B') has moved vertically towards the mouth plane of the cavity in the OC2 plane and is centred at y/h = -0.6. It is more clearly defined in this plane. The streamwise centre of the recirculation has also moved from x/l = 0.75 in the CL and OC1 planes to x/l = 0.93 in the OC2 plane. The size of recirculation 'B' is increased within the cavity, due to the change in shear layer behaviour close to the cavity sidewall compared with the CL and OC1 planes. The peak velocity magnitude within the cavity at the OC2 plane is approximately V = 100ms^{-1} (37% of freestream value). The peak velocity in the OC2 plane is significantly lower than in the CL and OC1 planes, because the shear layer is no longer deflected into the cavity allowing flow acceleration over recirculation 'A' but instead is elevated above the level of the mouth plane by the proximity to the sidewall. The peak vertical velocity in the OC2 plane is approximately v = ±30ms^{-1}, which occurs in the vertical motion regions of recirculation 'B' since the shear layer no longer impinges on the downstream wall leading to rapid vertical flow towards the cavity floor. In contrast, the structure of the flow in the numerical simulation OC2 plane is very similar to that seen in the OC1 and CL planes. The difference between the two cases can be attributed to the smaller shear layer deflection seen in the simulation. The flow recirculation is centred at x/l = 0.85, y/h = -0.49, which is

consistent with the x/l = 0.85 centre of recirculation seen on the sidewall streamlines (see Figure 7). The peak velocity in the OC2 plane is V = 95ms^{-1}, which is seen at x/l = 0.85 where the maximum shear layer deflection into the cavity occurs. The peak velocity is 18ms^{-1} lower than the peak velocities seen in the CL and OC1 planes. The peak vertical velocity in the OC2 plane is v = 75ms^{-1}, which is seen in the flow travelling along the downstream wall of the cavity towards the floor. This peak velocity is consistent with the values measured in the CL and OC1 planes.

Overall, the mean flow structure within the cavity in both cases is highly uniform across the CL and OC1 planes, with a single large recirculation present downstream of the 'tornado-like' vortices. The main flow difference between the two cases is evident in the OC2 plane where the experimental flow structure is changed due to the deeper shear layer deflection at the downstream wall. As with the previous experimental techniques, the PIV data shows the cavity to be exhibiting open/transitional-open behaviour compared with the open type flow seen in the simulation.

Discussion of Results

Each of the measurement techniques used to look at the different aspects of the flow i.e. pressure, structure etc. provides data which lead to the same conclusions about the type of flow which the cavity is exhibiting. Based on the definitions of flow types provided by Charwat *et al*. [11] and later by Stallings and Wilcox [12], the experimental cavity is shown to exhibit transitional-open flow behaviour with two flow recirculation regions in the cavity over which the shear layer passes. This contrasts with the open type flow exhibited by the numerical simulation, however, this has been attributed to the difference in shear layer behaviour between the two studies.

A strong oscillation feedback mechanism is present within the cavity. Both the experimental and numerical unsteady pressure spectra show the first three Rossiter modes of oscillation at frequencies which have excellent agreement with the theoretical values calculated using the 'modified-Rossiter' equation. The cavity flow is seen to oscillate in 1st mode dominance with a peak SPL value in 1st mode of approx 160dB in both cases.

The centreline flow plane is predominantly two-dimensional based on the oil flow streamline data but the flow becomes highly three-dimensional when moving from the centreline plane towards the cavity sidewalls due to the vertical flow structures within the cavity

The accuracy of the PIV measurements could be increased by using seeding particles with sub-micron diameters, however, this would then require greater laser power to scatter an equivalent amount of light, which was not possible for the present tests. The low-frequency PIV system used here is too slow to resolve fully the flow structure changes associated with the dominant frequencies of oscillation. At least a 2kHz system would be needed before time-resolved data could be acquired successfully.

Figure 11 shows a graphical representation of the three-dimensional flow within the l/h = 5 cavity which is constructed based on the flow information extracted from the experimental and numerical data collected within the cavity. The representation shows the flow structure through each of the three spanwise measurement planes and the flow structure as viewed from directly above the cavity. The representations use a topology defined by ESDU [13] in their review of time-averaged cavity flow behaviour.

Conclusions

The current study of an l/h=5 geometry cavity has used both experimental and numerical techniques to make detailed measurements of the flow behaviour within the cavity on and off the centreline plane. These measurements have confirmed the oscillation feedback mechanism present within aerodynamically-deep cavities and have also revealed the influence of boundary layer/shear layer behaviour on the resulting cavity flow.

The integration of different experimental techniques resulted in a level of synergy in the resulting data which allowed for a deeper understanding of the flow within the cavity. For example, the twin recirculation structure within the cavity could only be confirmed once the PIV measurements were completed as the surface flow

visualisations and pressure measurements were insufficient to identify these features. The same can be said when considering the interaction between experimental and numerical data. By combining the computational and experimental data we are able to produce validated, three-dimensional flow structures, such as that shown in Figure 11. These include the vertical vortical structures shown in green which were not previously confirmed by experimental techniques and required the addition input from the numerical simulation.

Although not reported here, similar techniques have also been used in other cavity geometries, and we have investigated the effect of representative stores at various locations in the cavity.

Acknowledgments

The authors would like to thank the UK's Engineering and Physical Sciences Research Council and MBDA UK Ltd for their support of the project under the Cooperative Awards in Science and Engineering studentship scheme.

References

1. East, L., *Aerodynamically Induced Resonance in Rectangular Cavities.* Journal of Sound and Vibration, 1966. **3**(3): p. 277-287.
2. Stallings, R.L., et al., *Measurements of Store Forces and Moments and Cavity Pressures for a Generic Store in and Near a Box Cavity at Subsonic and Transonic Speeds.* 1995, NASA-TM-4611.
3. Adrian, R.J., *Particle Imaging Techniques for Experimental Fluid Mechanics.* Annual Review of Fluid Mechanics, 1991(23): p. 261-304.
4. Durao, D., J. Pereira, and J. Sousa. *LDV Measurements of Turbulent Separated Flow Over a Cavity*. in *6th International Symposium on the Applications of Laser techniques to Fluid Mechanics*. 1992. Lisbon, Portugal.
5. Ross, J., A. *Measurement of the Flow within an Aerodynamically Deep Weapons Bay using Particle Image Velocimetry* in *RAeS Internal Weapons Carriage and Release Conference*. 2004. Boscombe Down, UK.
6. Scarano, F., *Iterative Image Deformation Methods in PIV.* Measurement Science Technology, 2002(13): p. 1-19.
7. Grace, S.M., *An Overview of Computational Aeroacoustics Techniques Applied to Cavity Noise Prediction.* in *39th AIAA Aerospace Sciences Meeting and Exhibit*. 2001 Reno, NV.
8. Shih, T.H, Liou, W.W., Shabbir, A., Yang, Z., and Zhu, J. *A New k-e Eddy Viscosity Model for High Reynolds Number Turbulent Flows – Model Development and Validation*. Computers and Fluids 1995. **24**: p227-238.
9. Rossiter, J.E., *Wind Tunnel Experiments on the Flow Over Rectangular Cavities at Subsonic and Transonic Speeds.* Royal Aircraft Establishment, Farnborough, UK (ARC R&M 3438)
10. Hunt, J.C.R., Abell, C.J., Peterka, J.A. and Woo, H. *Kinematical studies of the flows around free or surface-mounted obstacles; applying topology to flow visualization*, J. Fluid Mech. 1978. **86:** p. 179–200.
11. Charwat, A.F., et al., *An Investigation of Separated Flows - Part 1 : The Pressure Field.* Journal of Aerospace Sciences, 1961a. **28**(6): p. 457-470.
12. Stallings, R.L. and F.J. Wilcox, *Experimental Cavity Pressure Distributions at Supersonic Speeds*. 1987, NASA-TP-2683.
13. ESDU, *Drag of a Rectangular Planform Cavity in a Flat Plate with a Turbulent Boundary Layer for Mach Numbers up to 3. Part II : Open and transitional flows*. 2002, ESDU.

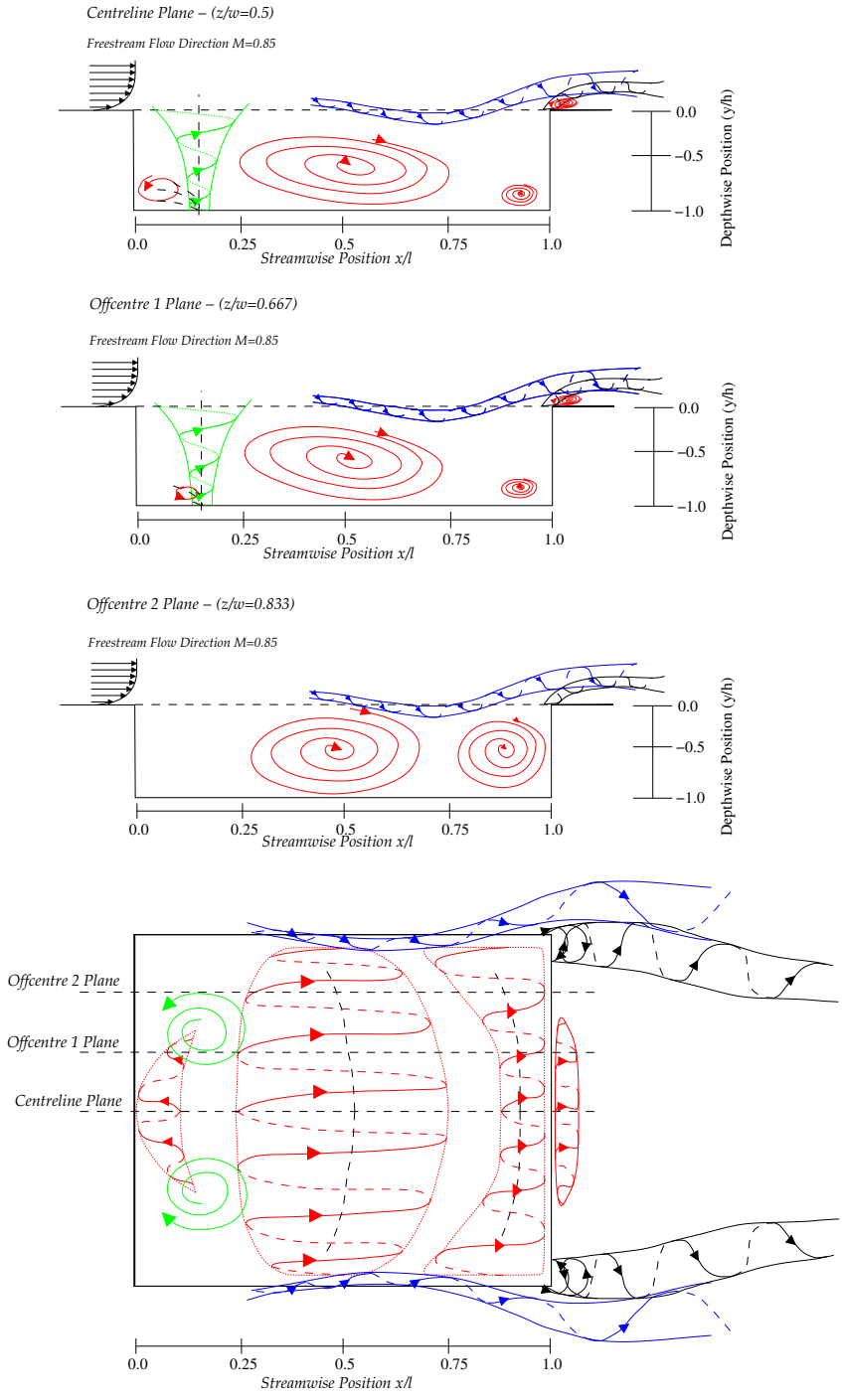

Figure 11. Graphical Interpretation of Three-Dimensional Flow within an l/h=5 Cavity

DEFENCE ACADEMY
OF THE UNITED KINGDOM
Cranfield UNIVERSITY
Defence College of Management and Technology

An Experimental and Computational Investigation of a 3D, l/h=5 Transonic Cavity Flow

Prof Kevin Knowles
Dr Simon Ritchie
Dr Nick Lawson

Overview

- Background
- Experimental Studies
- Computational Studies
- Results & Discussion
  - 3-D and unsteady features
- Conclusions

Cavity Flow Types

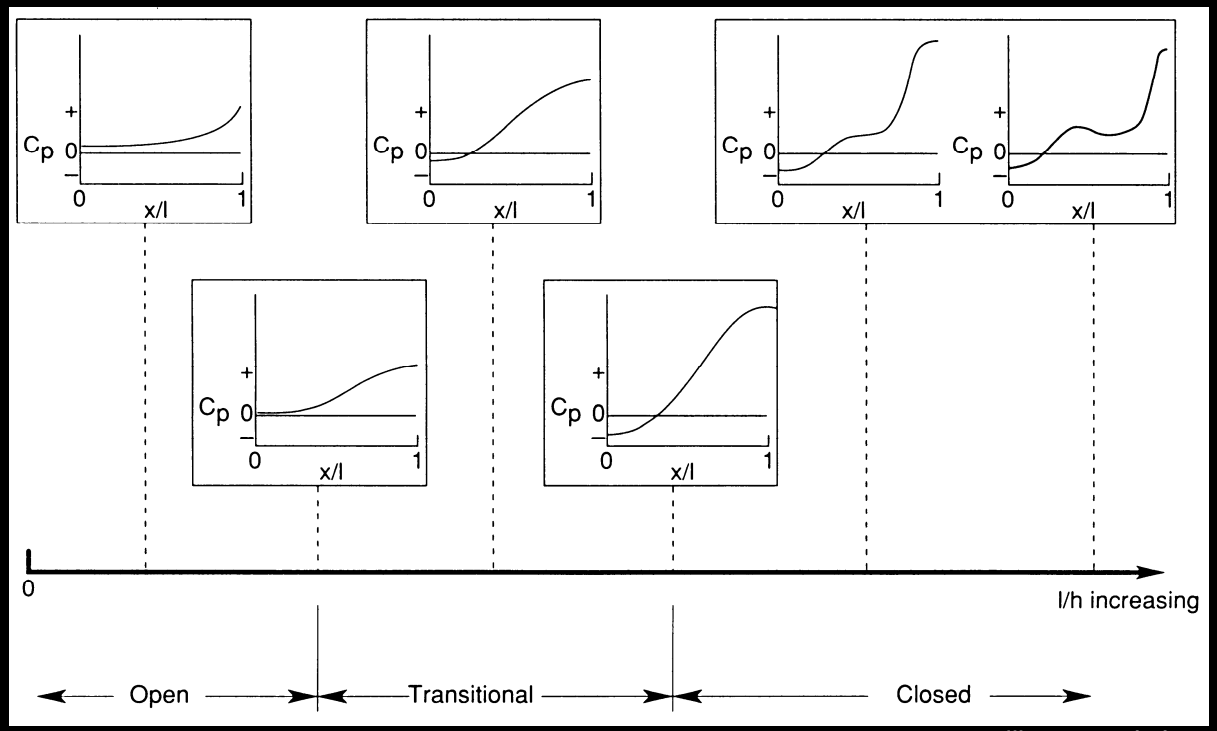

Stallings *et al (1994)*

There are three types of cavities, classified according to their *pressure distribution* and *flow behaviour*; the length/depth (l/h) ratio is the measure used for classification.

‘Open’ Cavity Flow

- Classified as cavities with l/h ratio less than 10.
- Open flow is characterised by self-sustained interactions between shear layer and vortices within the cavity.
- Tones can exceed 170dB

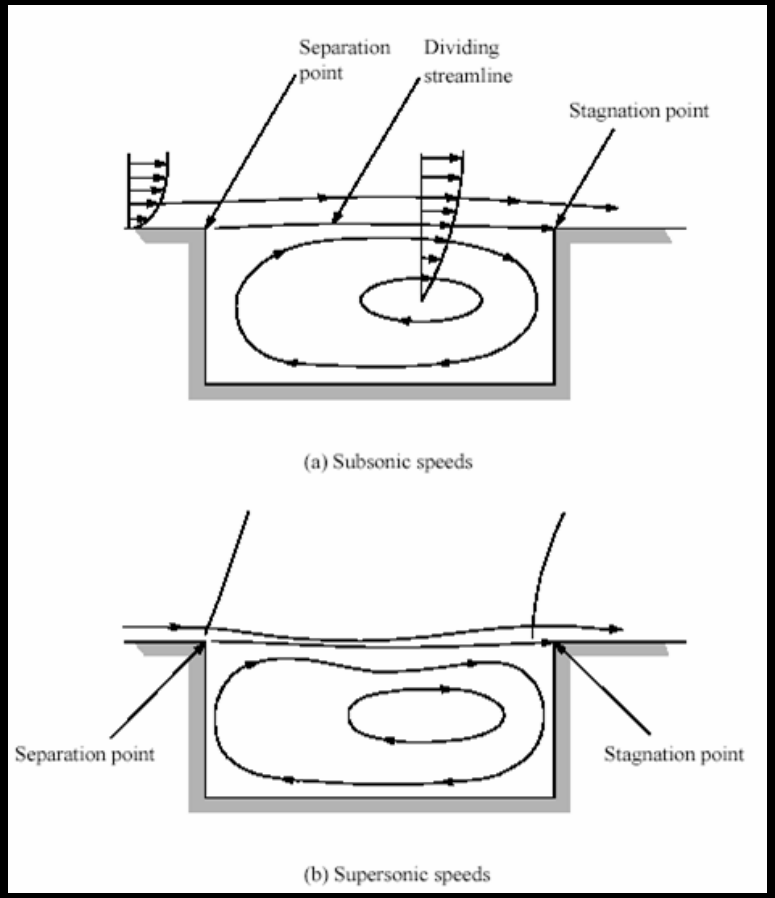

ESDU (2002)

‘Closed’ Cavity Flow

- Classified as cavities with l/h ratio greater than 13
- Closed cavity flow characterised by strong longitudinal pressure gradients within the cavity

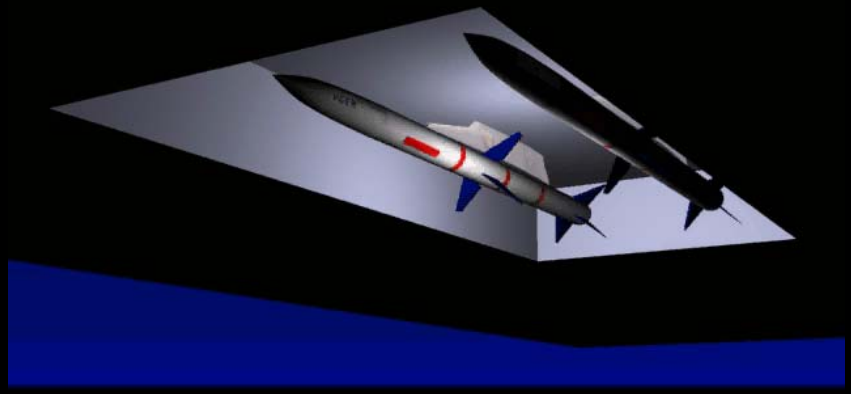

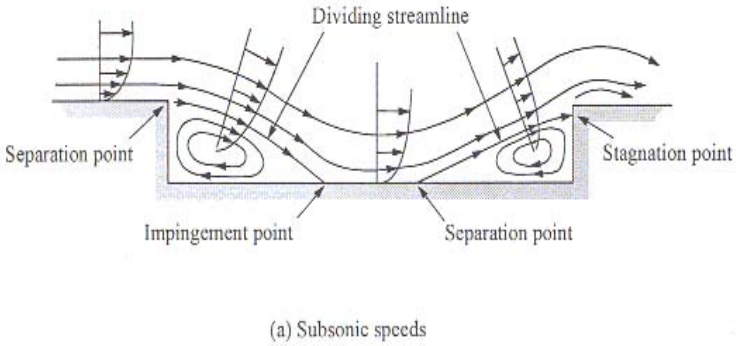

(a) Subsonic speeds

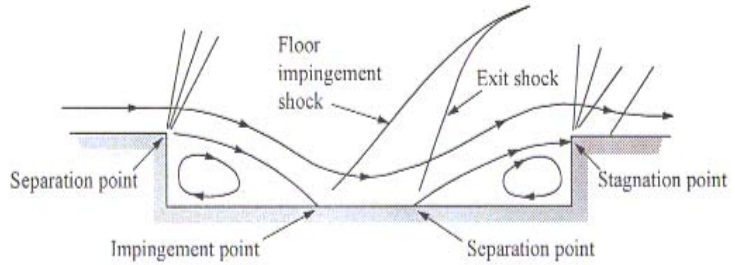

(b) Supersonic speeds

ESDU (2002)

Knowles et al

Background at Shrivenham

Non-intrusive Measurements

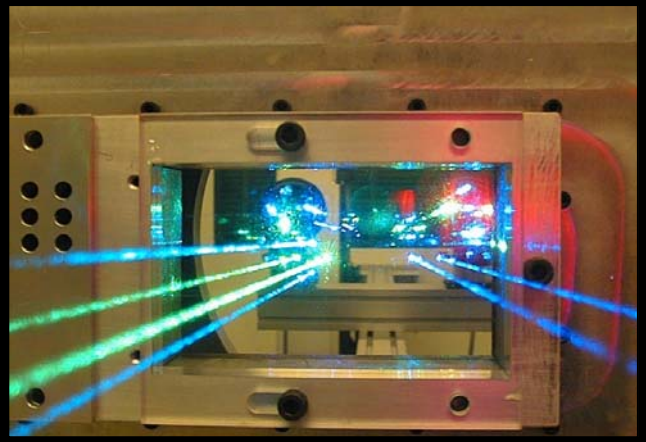

Flow visualisation

Pressure measurements

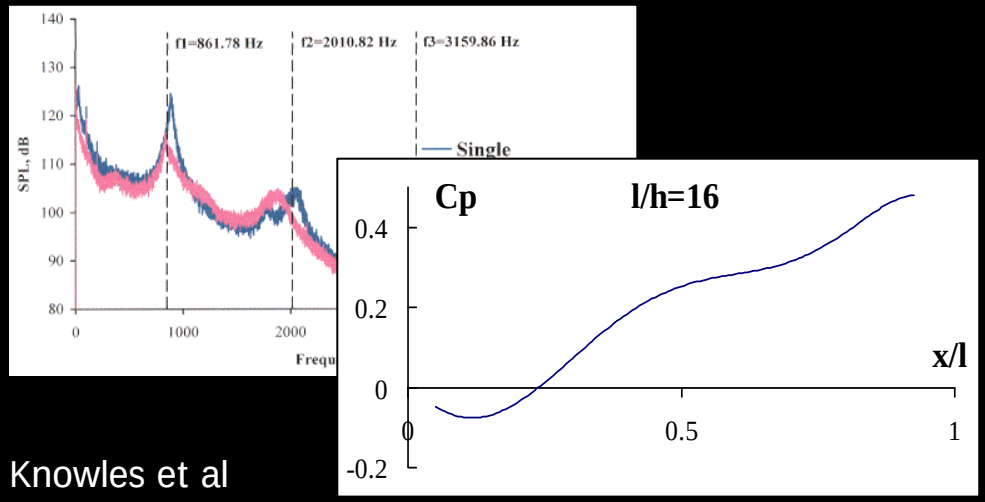

Knowles et al

CFD

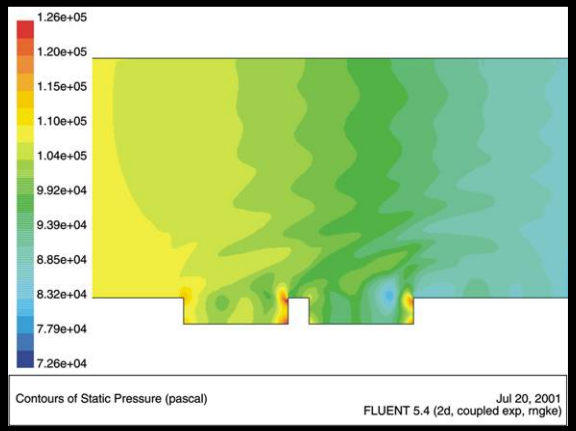

Laser Doppler Anemometry (LDA)

- LDA is a non-intrusive optical measurement technique for point wise velocity investigation
- Technique can be used in any gas or liquid flow
- Very high accuracy velocity and turbulence data for all 3 velocity components
- Time intensive technique – especially in intermittent and blow down facilities

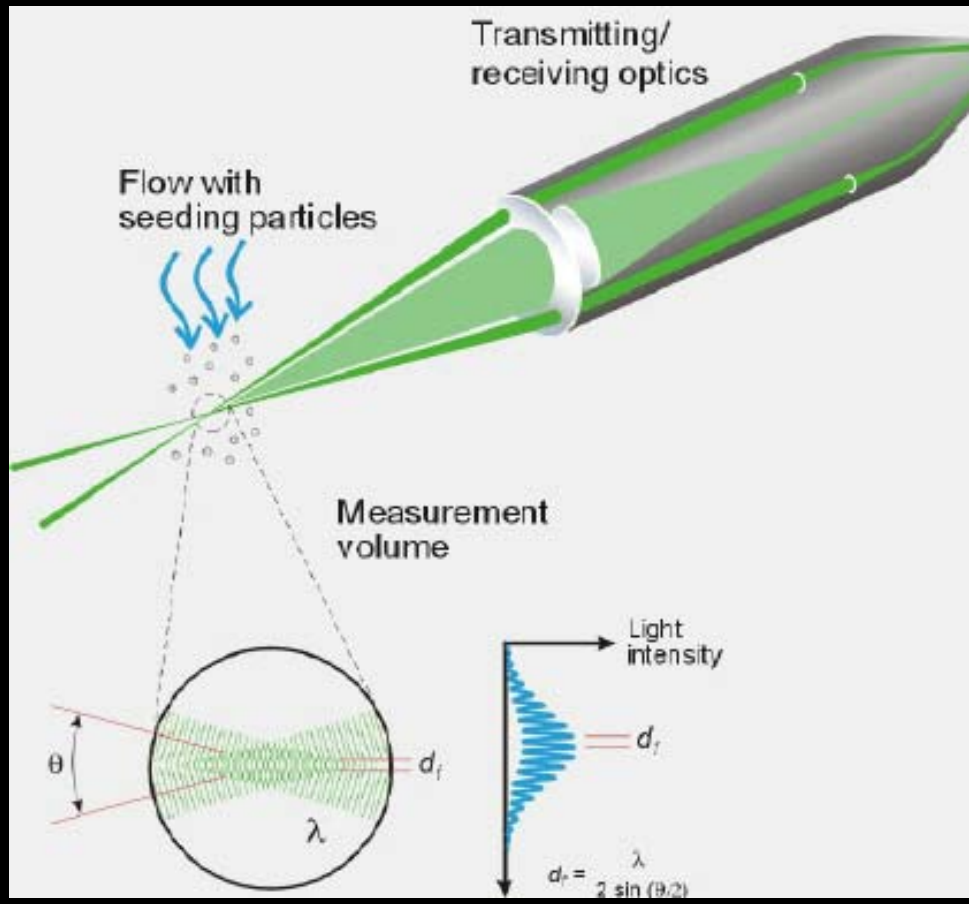

Dantec Dynamics

Knowles et al

Laser Doppler Anemometry (LDA)

- l/h=10 cavity
- $U_{inf}=20ms^{-1}$
- The data at each point are the mean of 5000 samples at 1kHz sampling rate

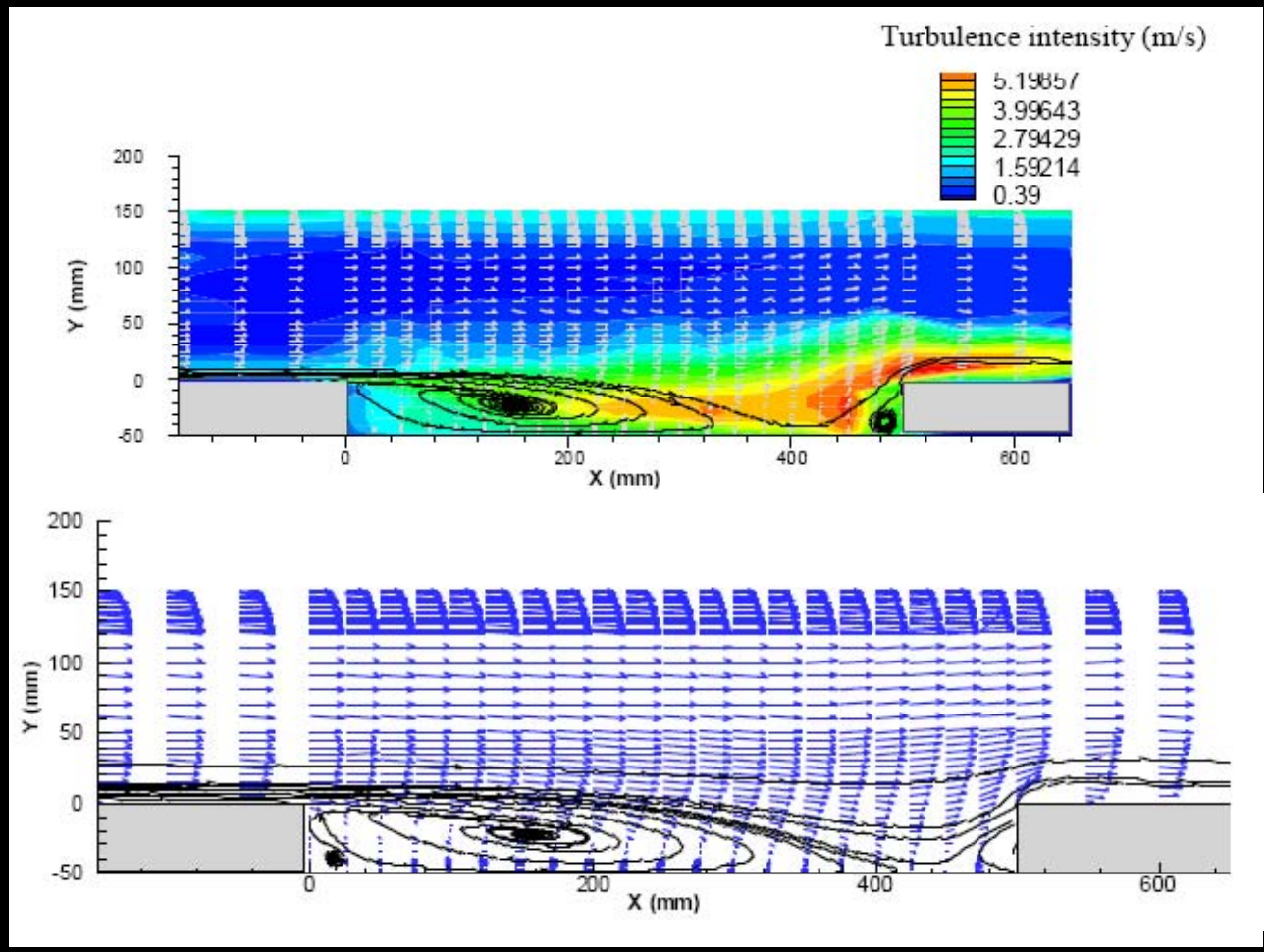

Esteve *et al (2000)*

Knowles et al

Particle Image Velocimetry (PIV)

- PIV is a non-intrusive optical measurement technique for whole field velocity and flow structure investigation
- Technique can be used in any gas or liquid flow
- Measurements in 2D or 3D
- Very quick data acquisition is attainable
- Technique requires plenty of optical access in order to be successful

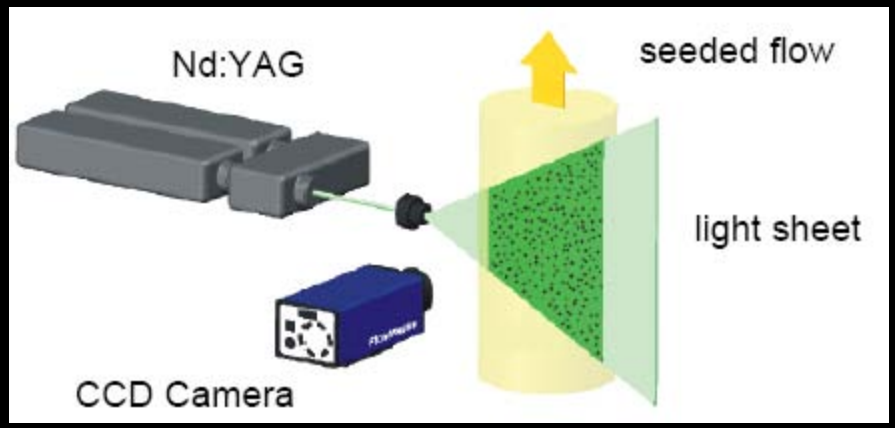

www.piv.de

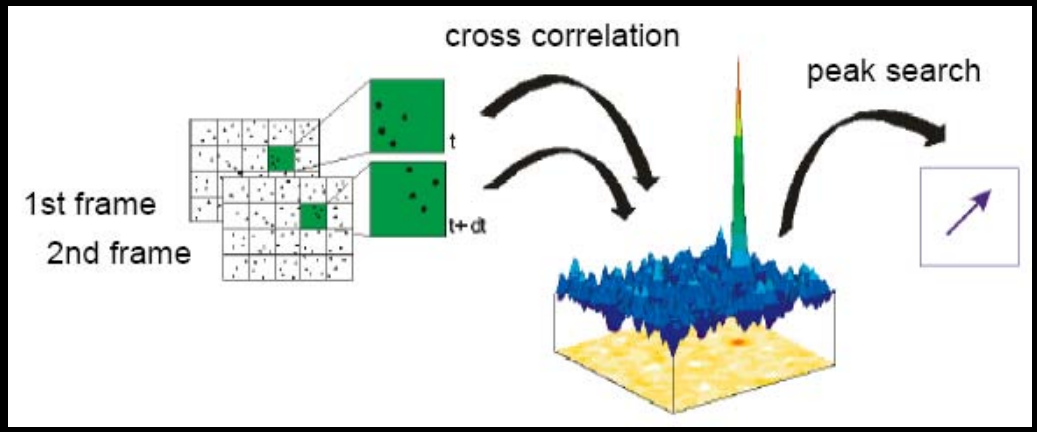

www.piv.de

Knowles et al

Guidelines for Flow Seeding

- Seeding must be homogeneous
- Particles must be small enough to accurately follow the flow, but large enough to scatter sufficient light for good images
- Seeding concentration must be controlled to prevent over-exposure or under-exposure of images
- Typical seeding materials tested – Water
  5% Glycerol in Water
  TiO_2 Powder

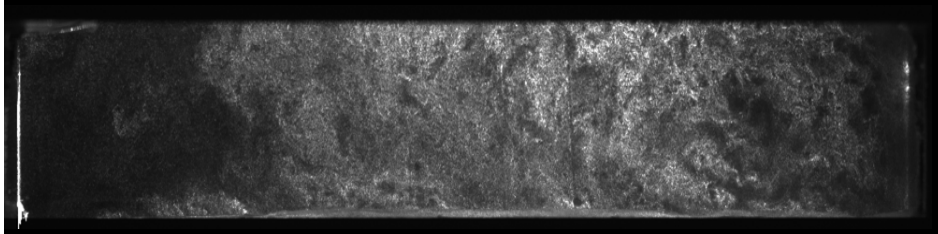

Over-exposed Image

Under-exposed Image

Knowles et al

Details of Test Cases

Open Cavity Case – l/h=5

Closed Cavity Case – l/h=14

- Cavity Length=160mm
- Cavity Width=80mm
- Cavity Depth=32mm and 11.4mm
- Test Mach Number=0.85
- Test Unit Reynolds Number=12.87×10^6 m^{-1}

Experimental Layout

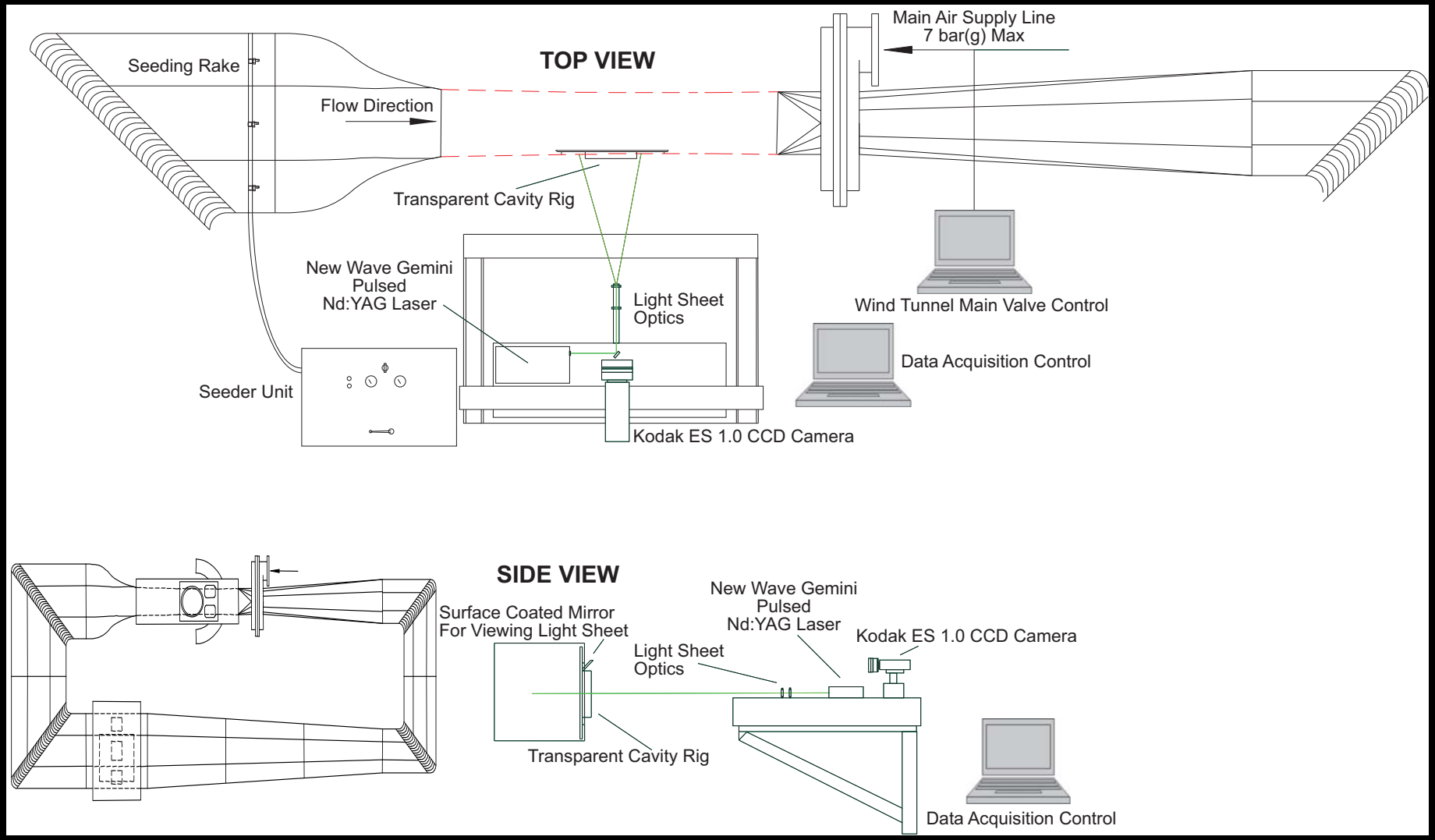

Cavity Rig for Experimental Study

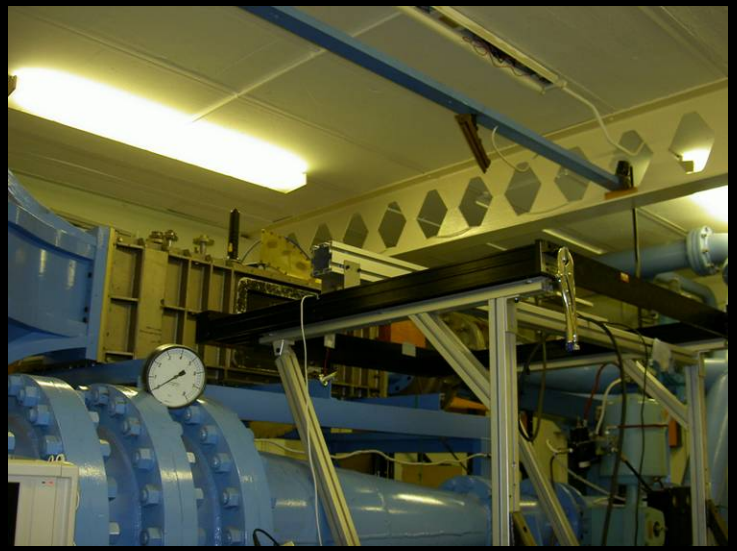

Laser and Camera Traverse

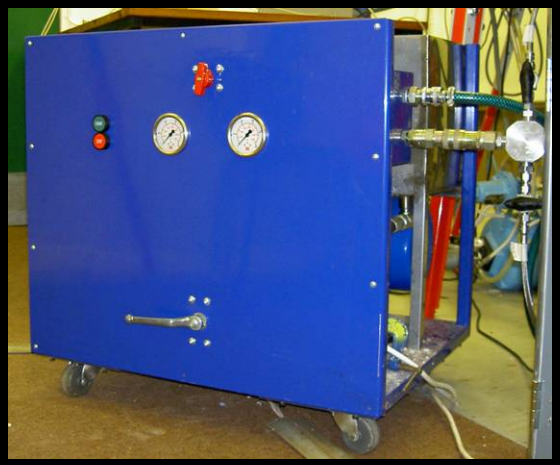

Custom Built Seeder

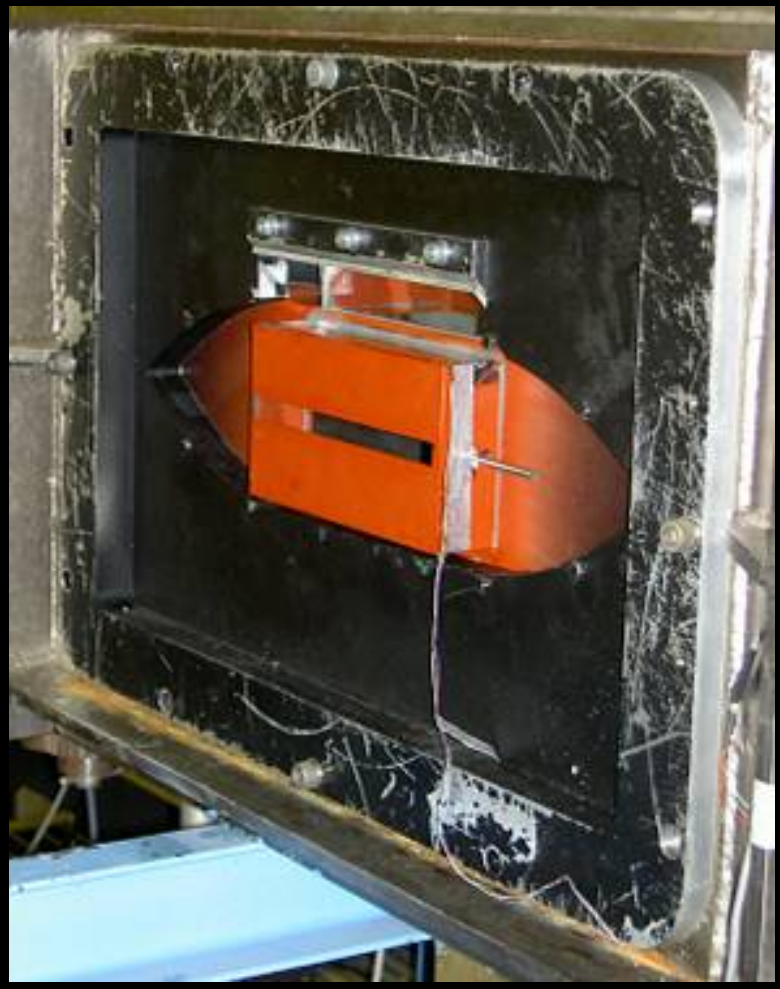

l/h=5 Cavity Rig Attachment

Knowles et al

Experimental Work

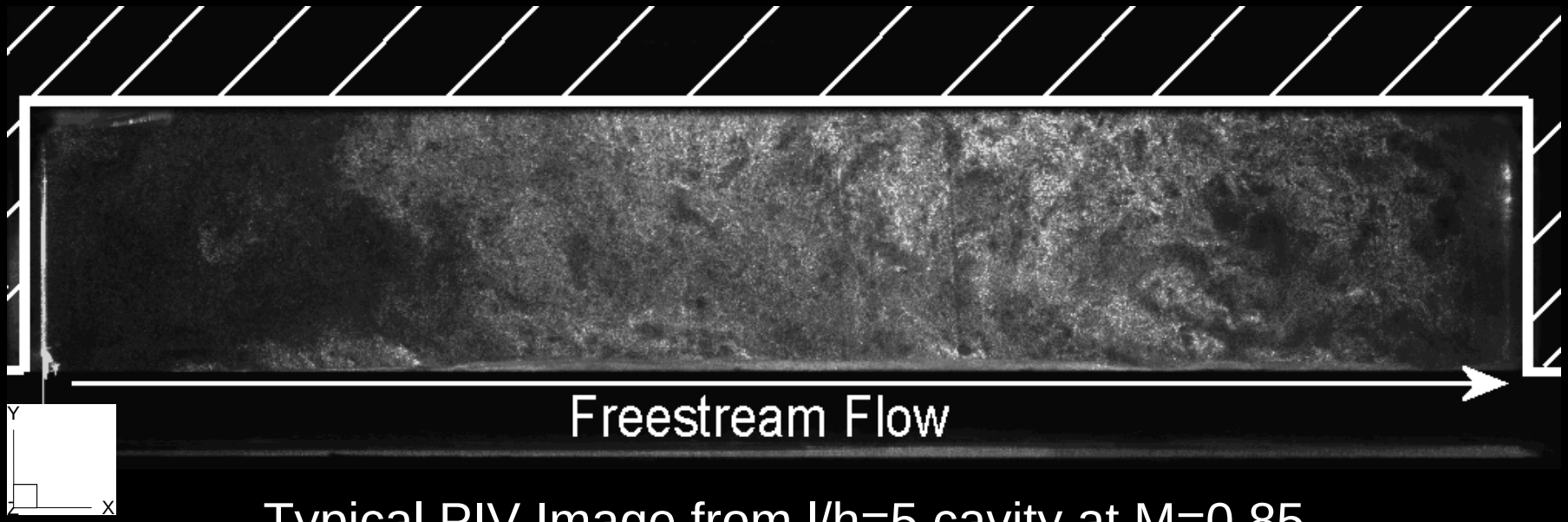

Typical PIV Image from l/h=5 cavity at M=0.85

Seeding : Water particles of 5-10μm diameter

Computational Domain

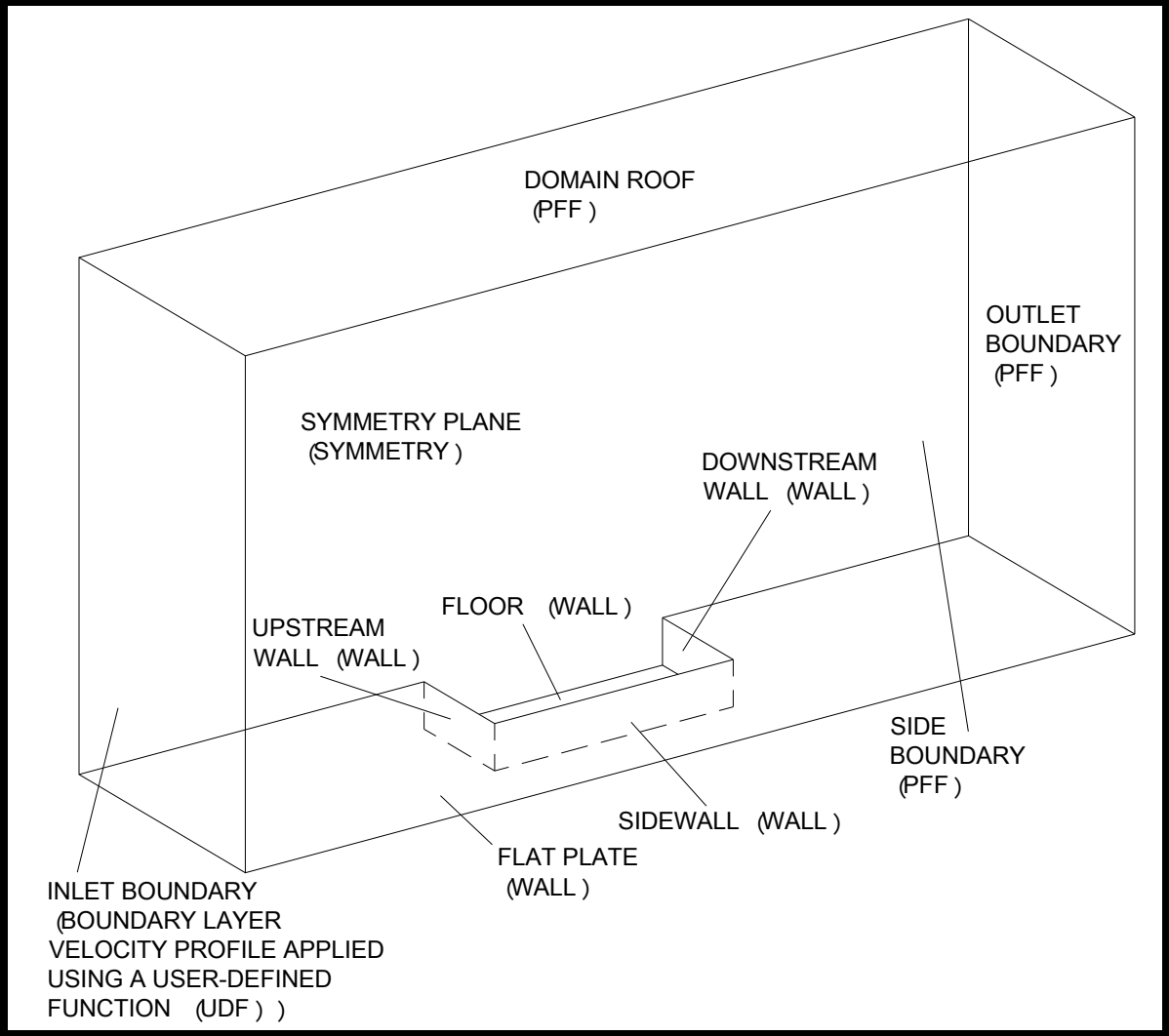

Cavity Animation (l/h=5)

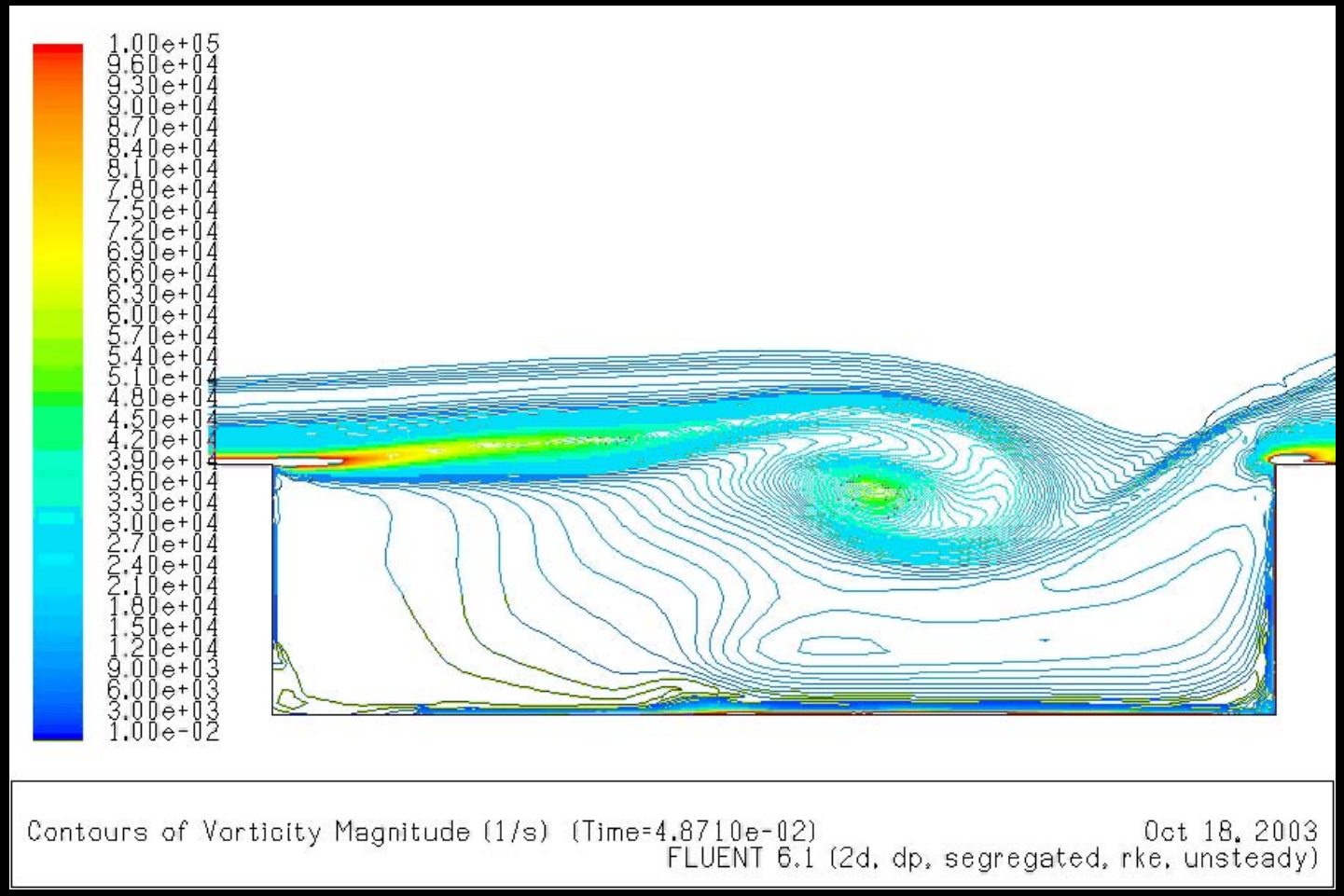

Contours of Vorticity Magnitude

Floor Pressure Distribution (l/h=4, M=0.91)

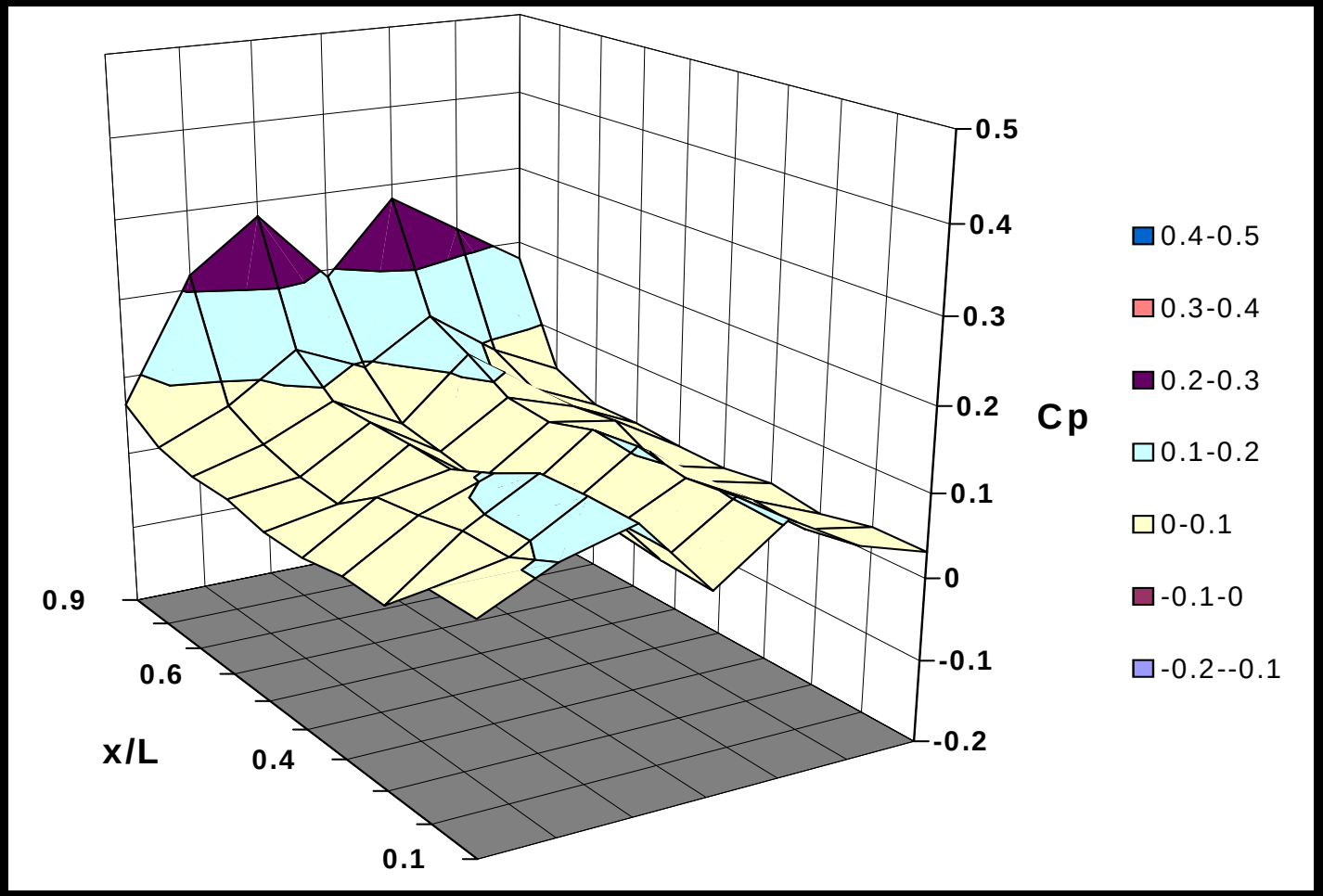

Floor Pressure Distribution (l/h=16, M=0.91)

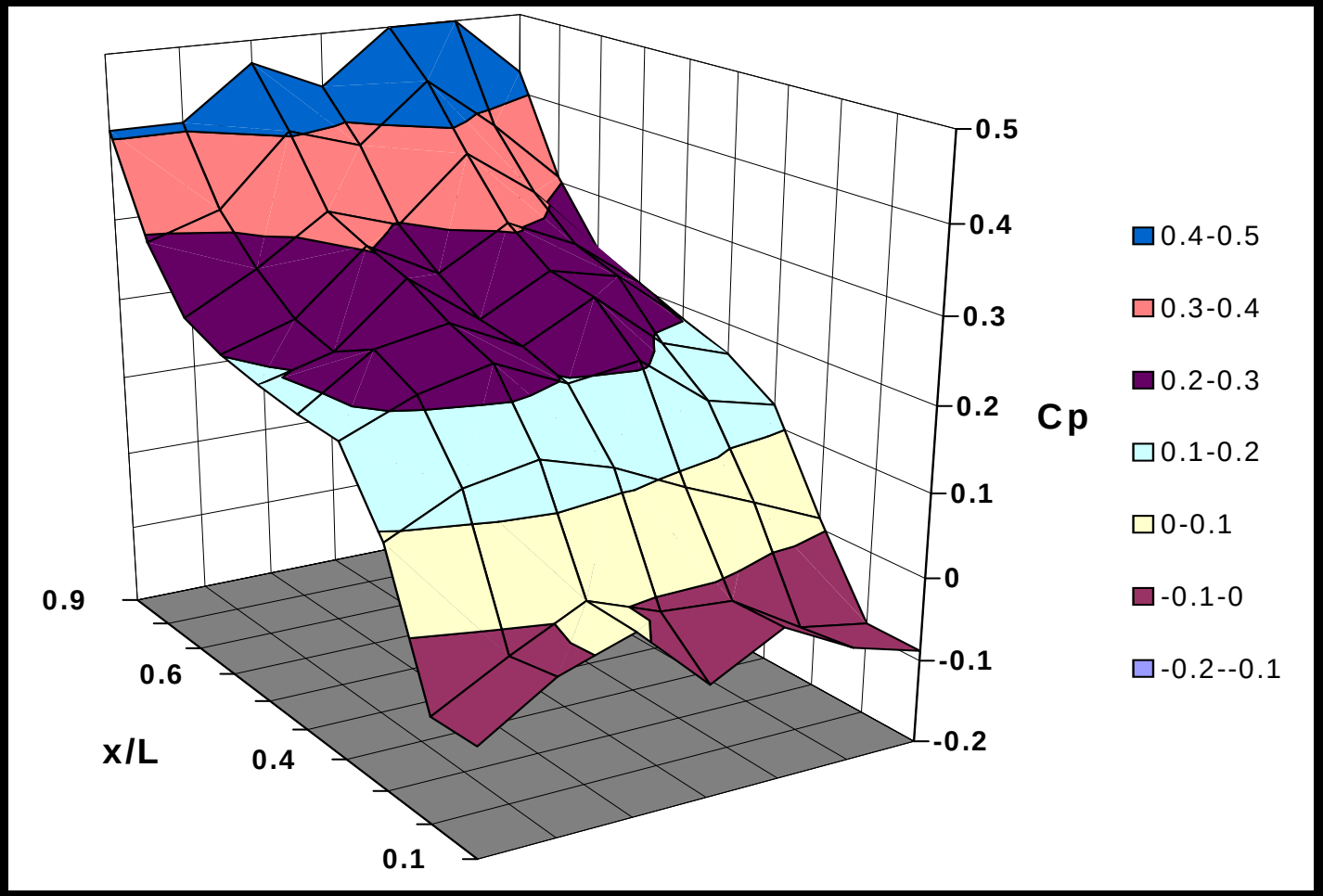

Evolution of Vortical Structures (DES simulation, l/h=4, M=0.91)

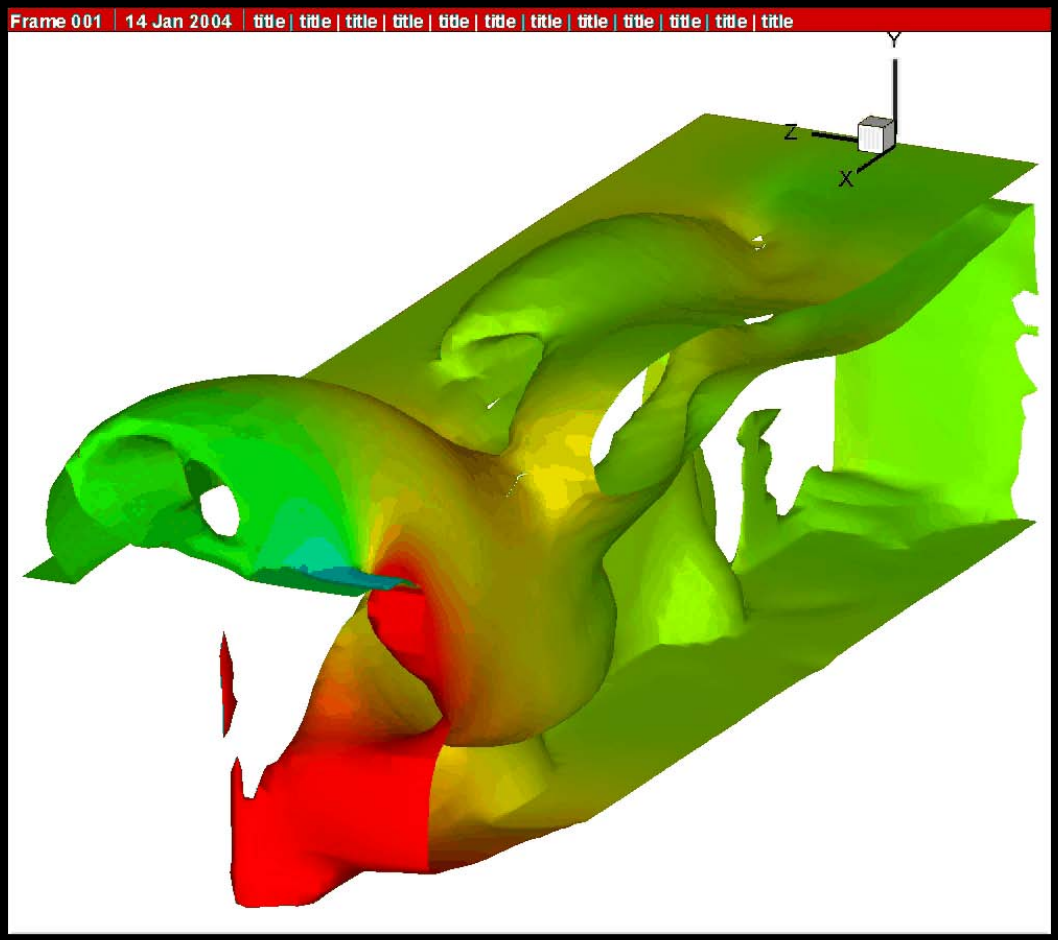

Knowles et al

Results – mean pressures

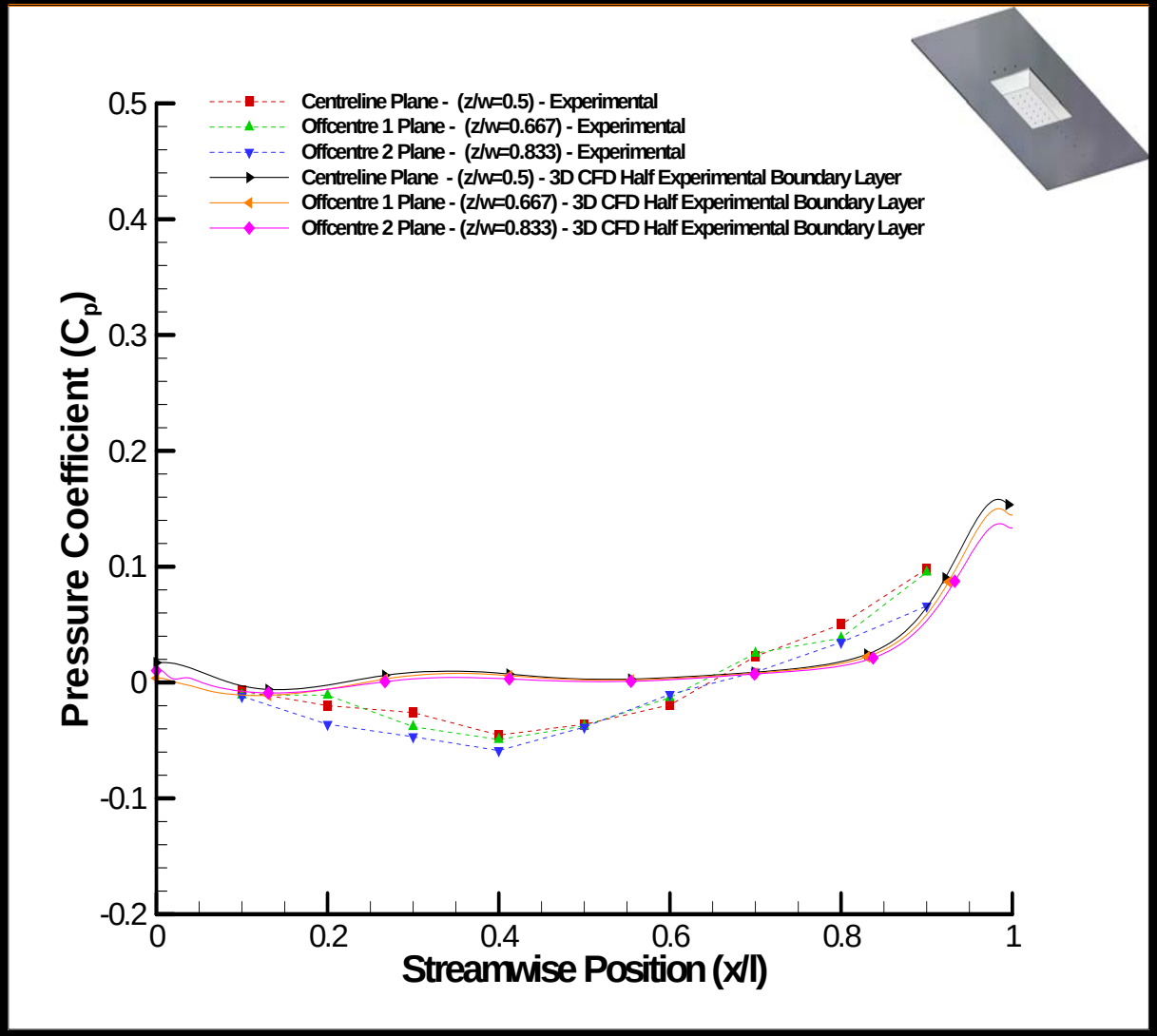

Results – unsteady pressures

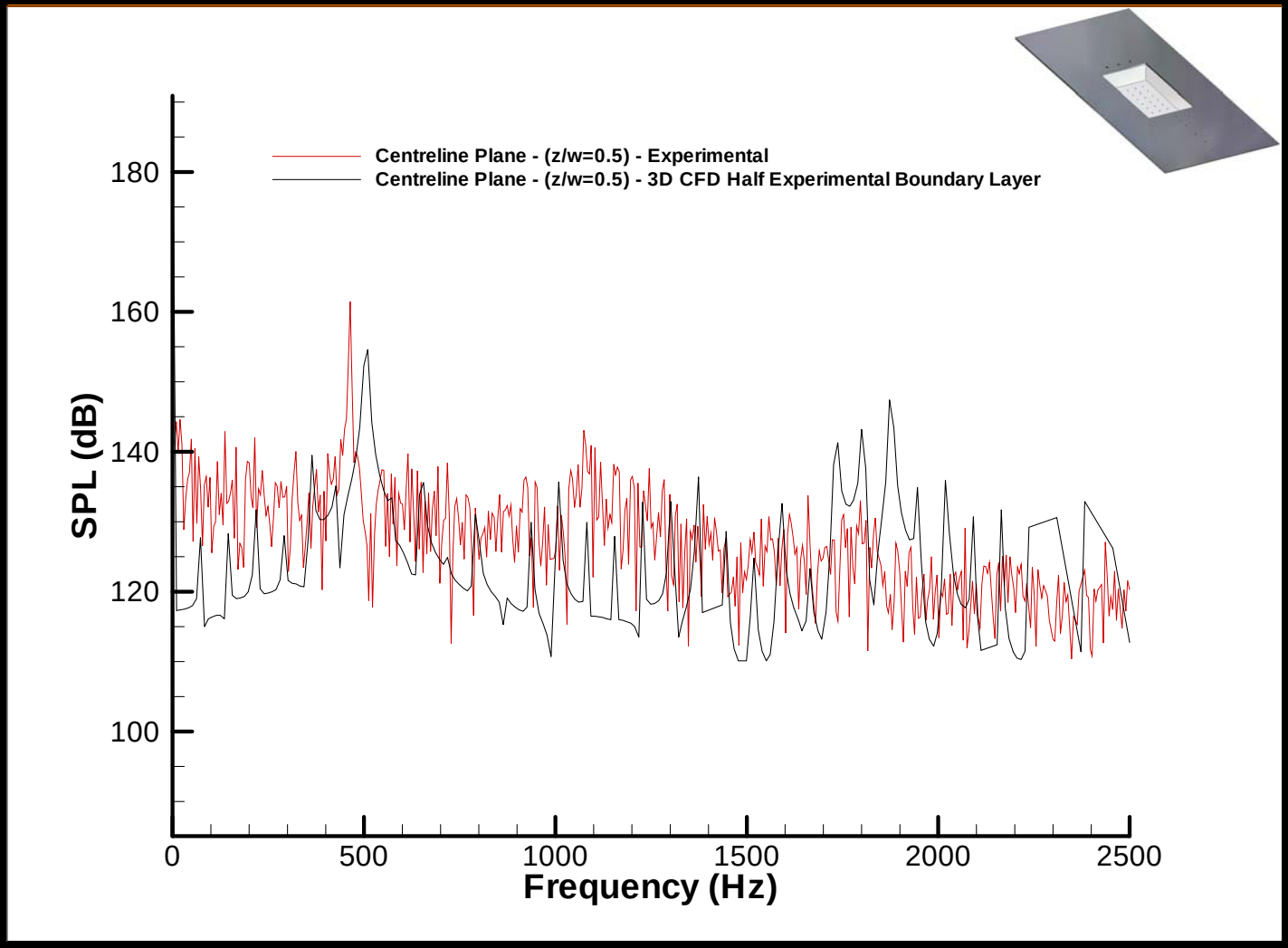

Results – flow visualisation

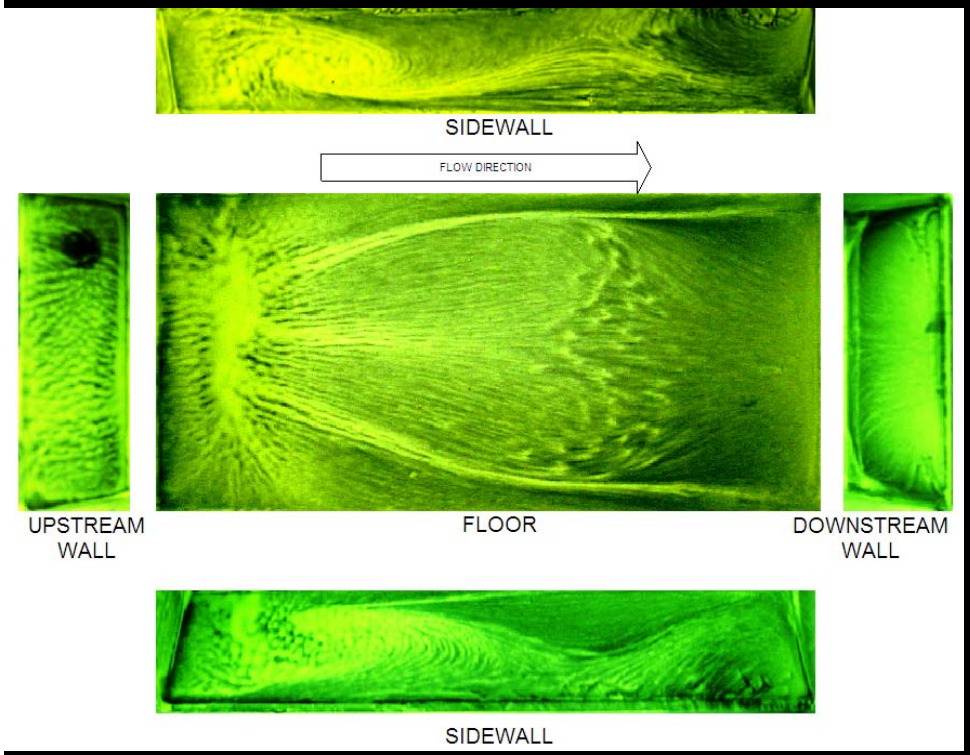

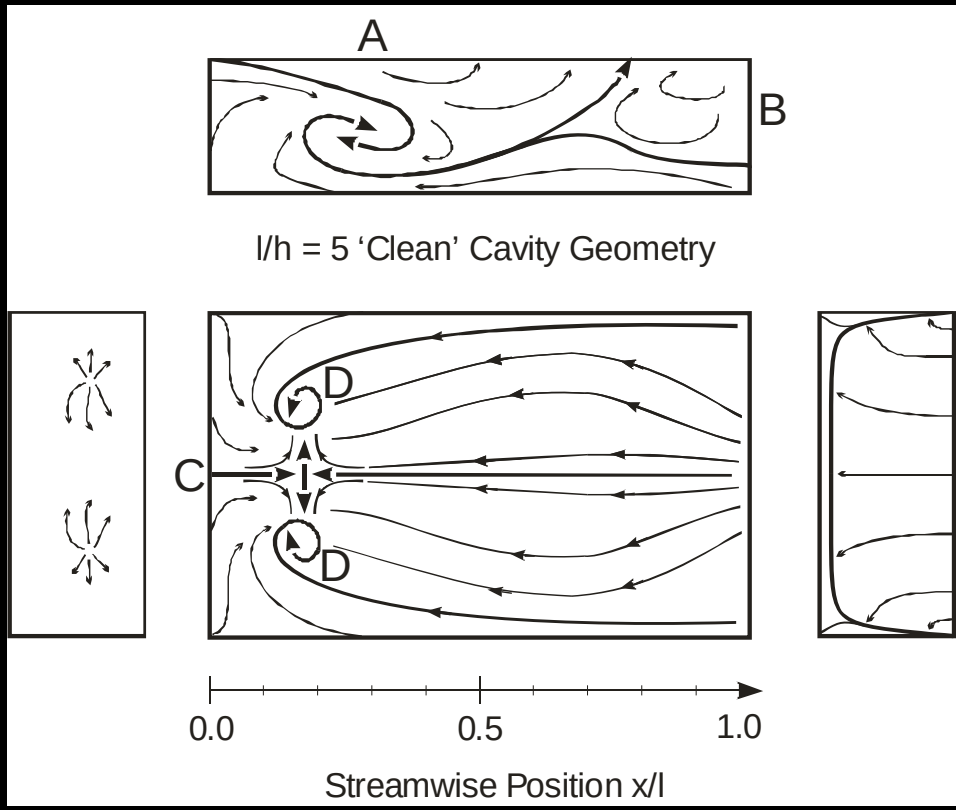

Results – CFD flow visualisation

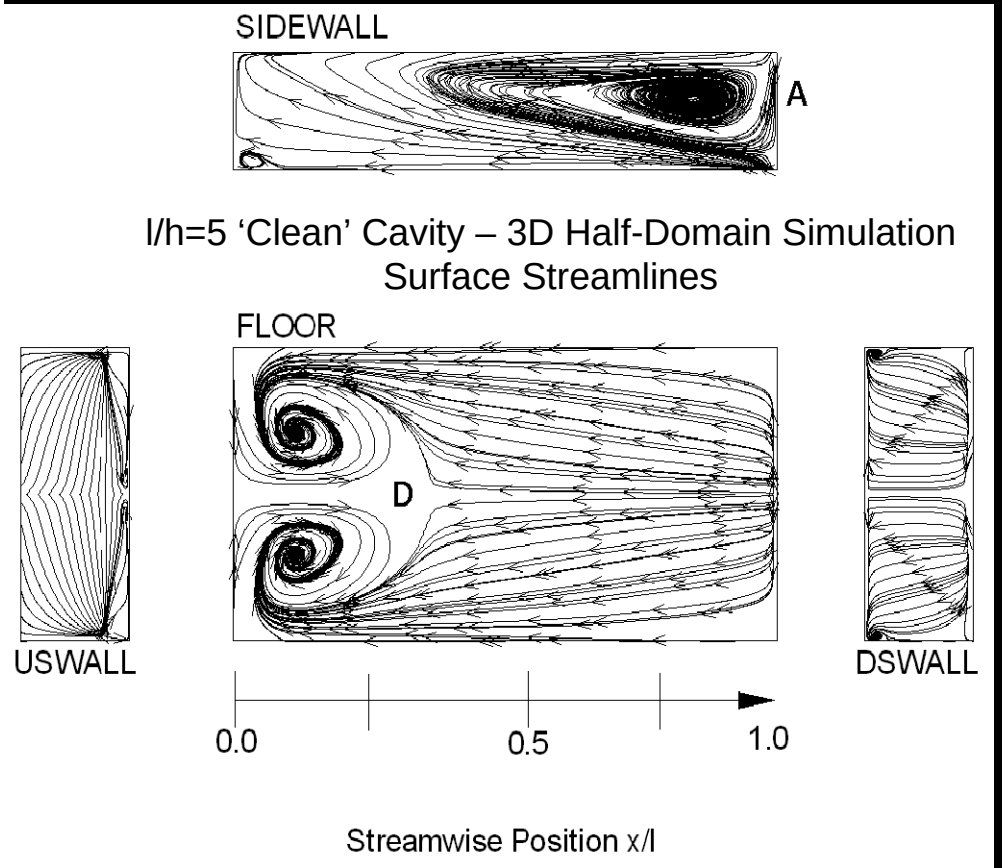

l/h=5 'Clean' Cavity – 3D Half-Domain Simulation
Surface Streamlines

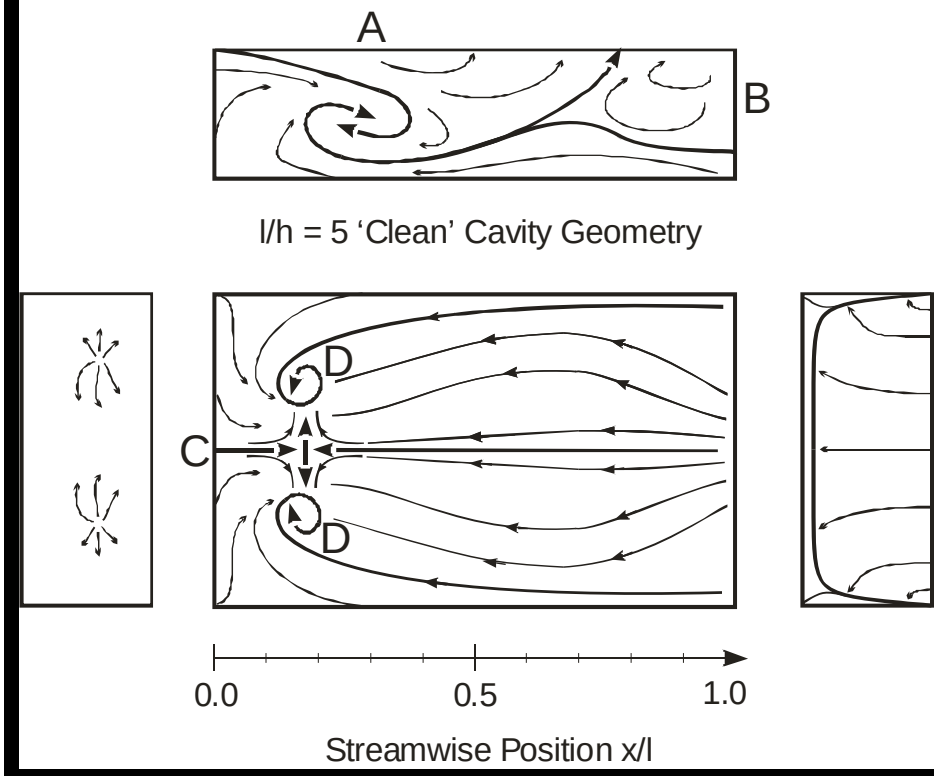

l/h = 5 'Clean' Cavity Geometry

Results – time-averaged velocity

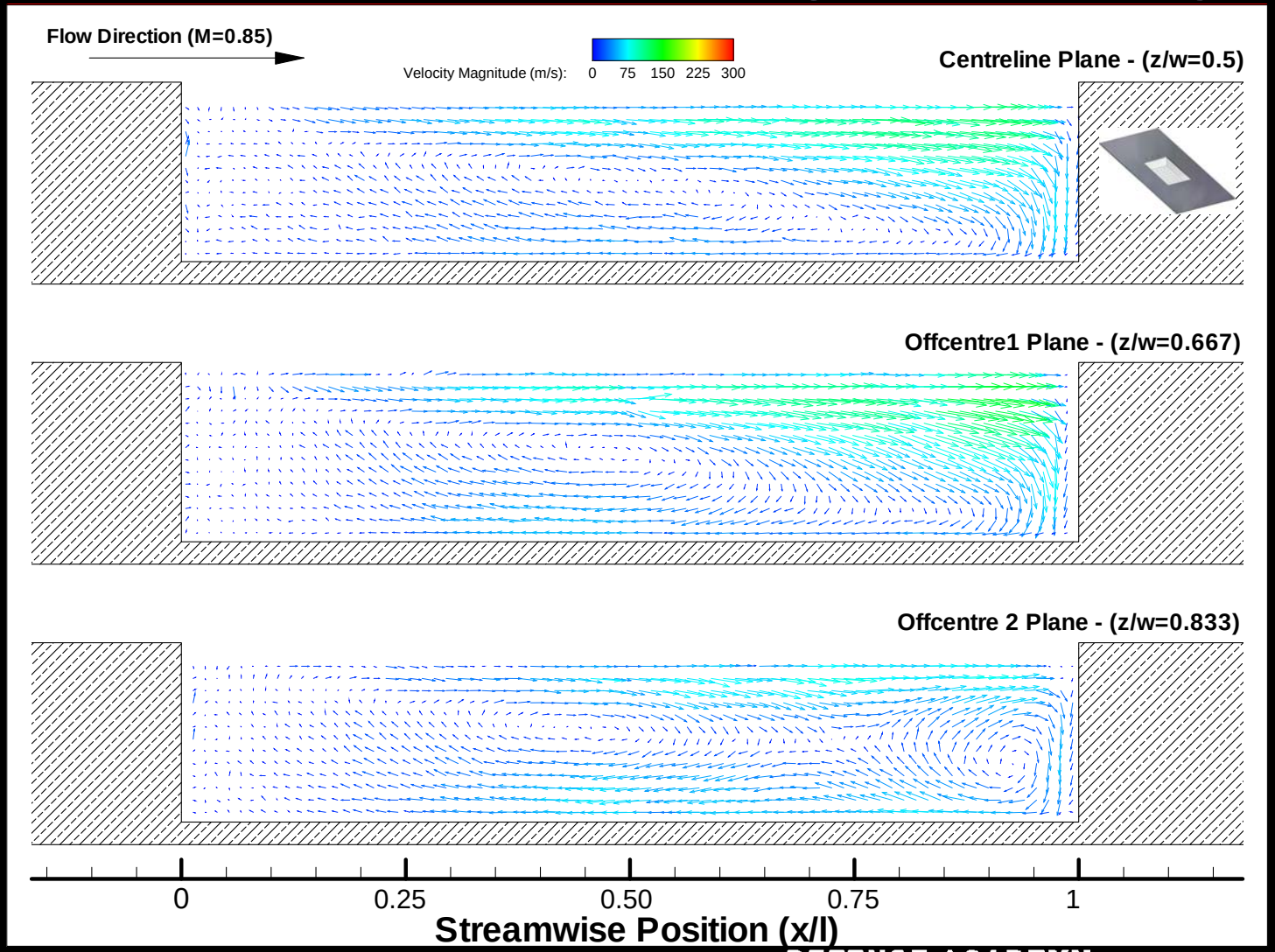

Results – CFD time-averaged velocity

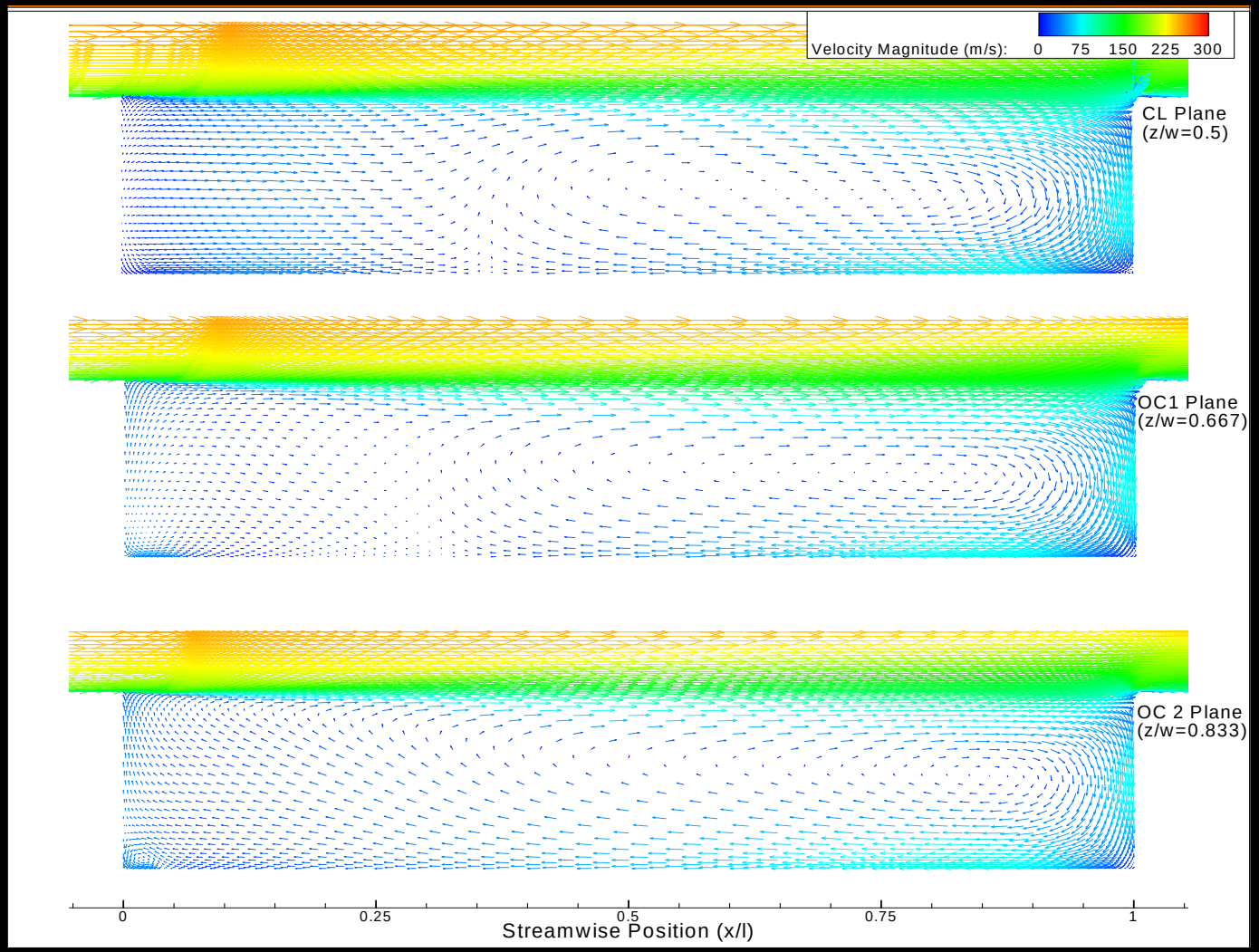

Knowles et al

Results – 3D flowfield

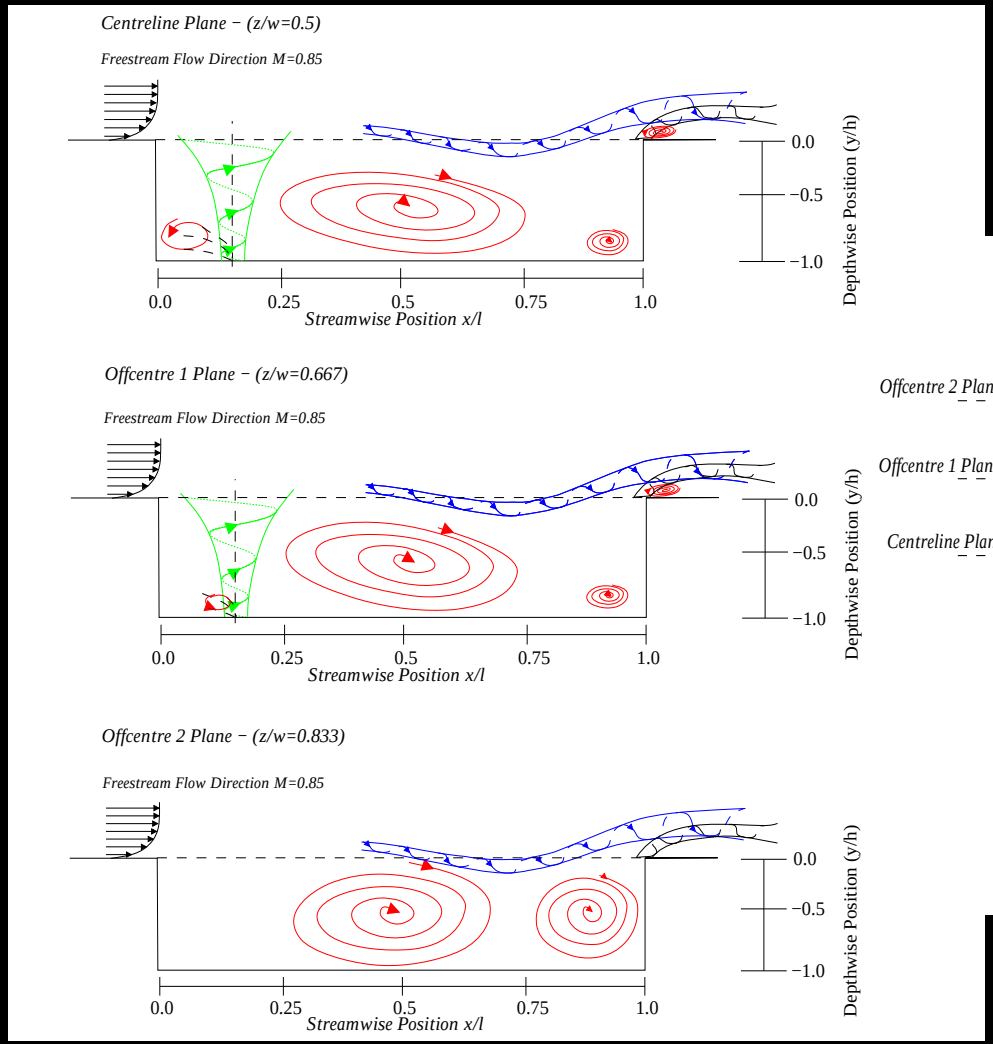

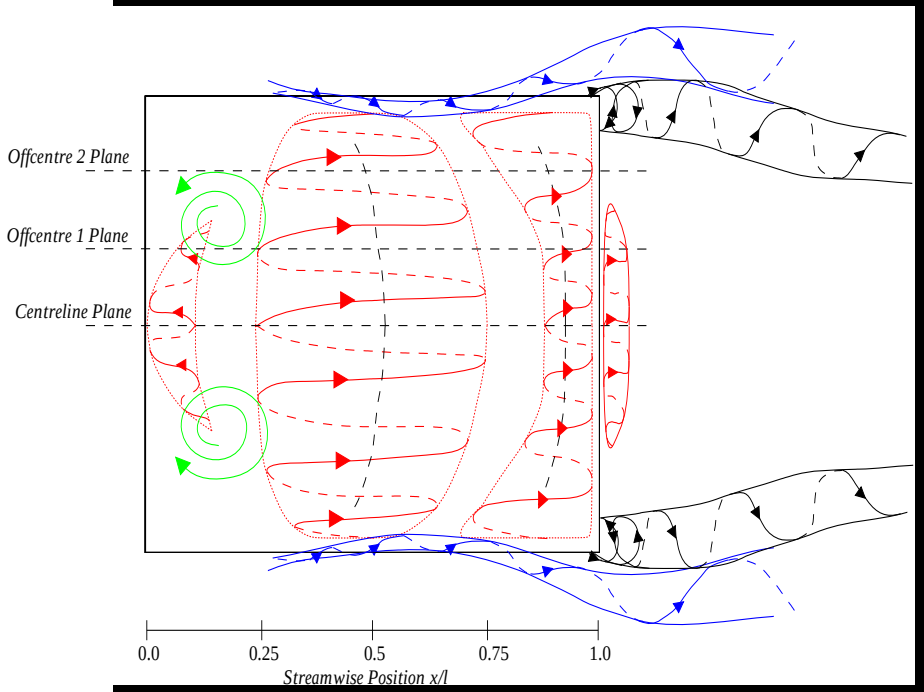

Knowles et al

DEFENCE ACADEMY
OF THE UNITED KINGDOM
Cranfield UNIVERSITY
Defence College of Management and Technology

Details of Missile Test Cases

Test Configurations (6 in total)

‘Clean’ Cavity

1 Missile on Centreline - 1MCL

1 Missile (Offcentre) – 1MOC

2 Missiles (CL and Offcentre) – 2MCLOC

2 Missiles (Offcentre) – 2MOC

3 Missiles (CL and Offcentre) – 3Missiles

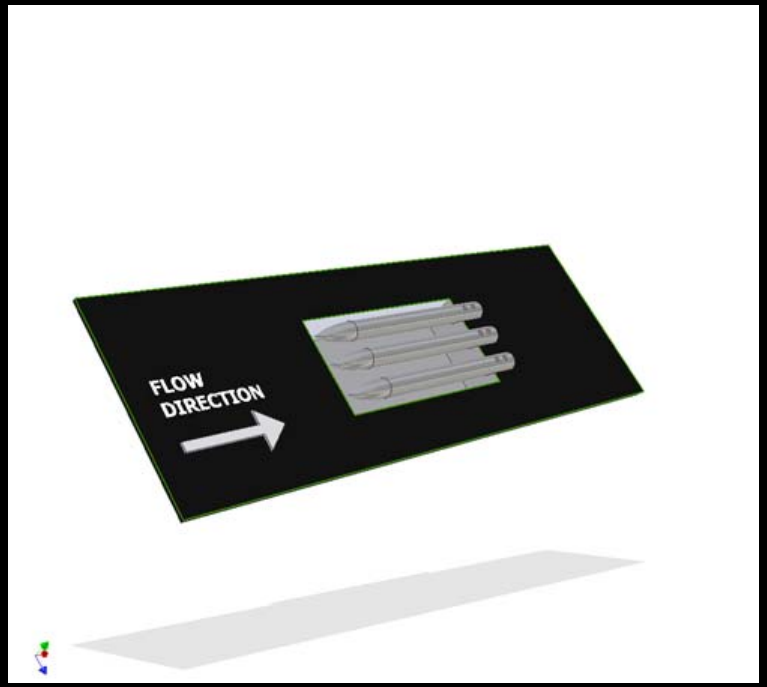

Only ‘Clean’, 1MCL and 3Missiles data are presented here

Flow visualisation with missiles

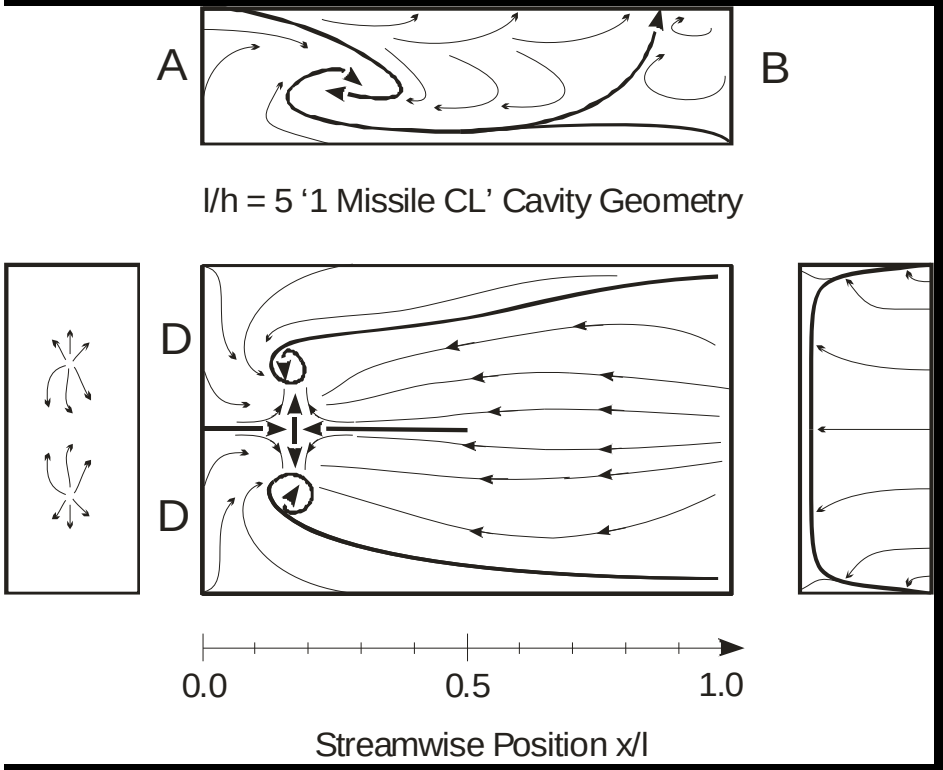

l/h = 5 '1 Missile CL' Cavity Geometry

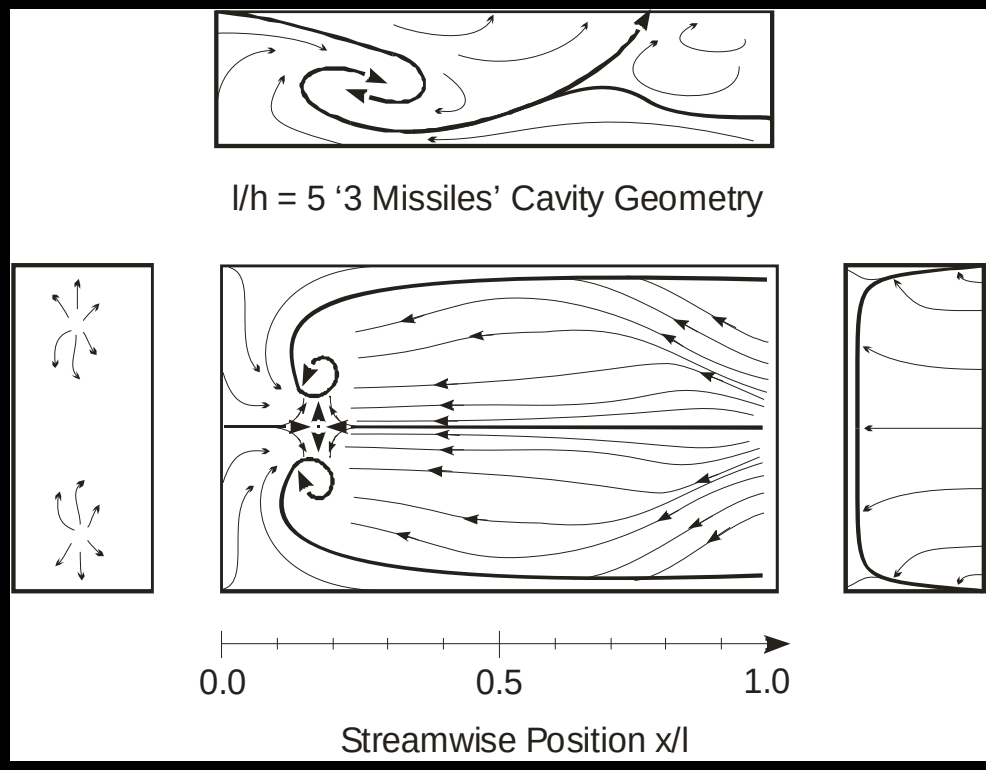

l/h = 5 '3 Missiles' Cavity Geometry

Centreline velocities – 1 missile

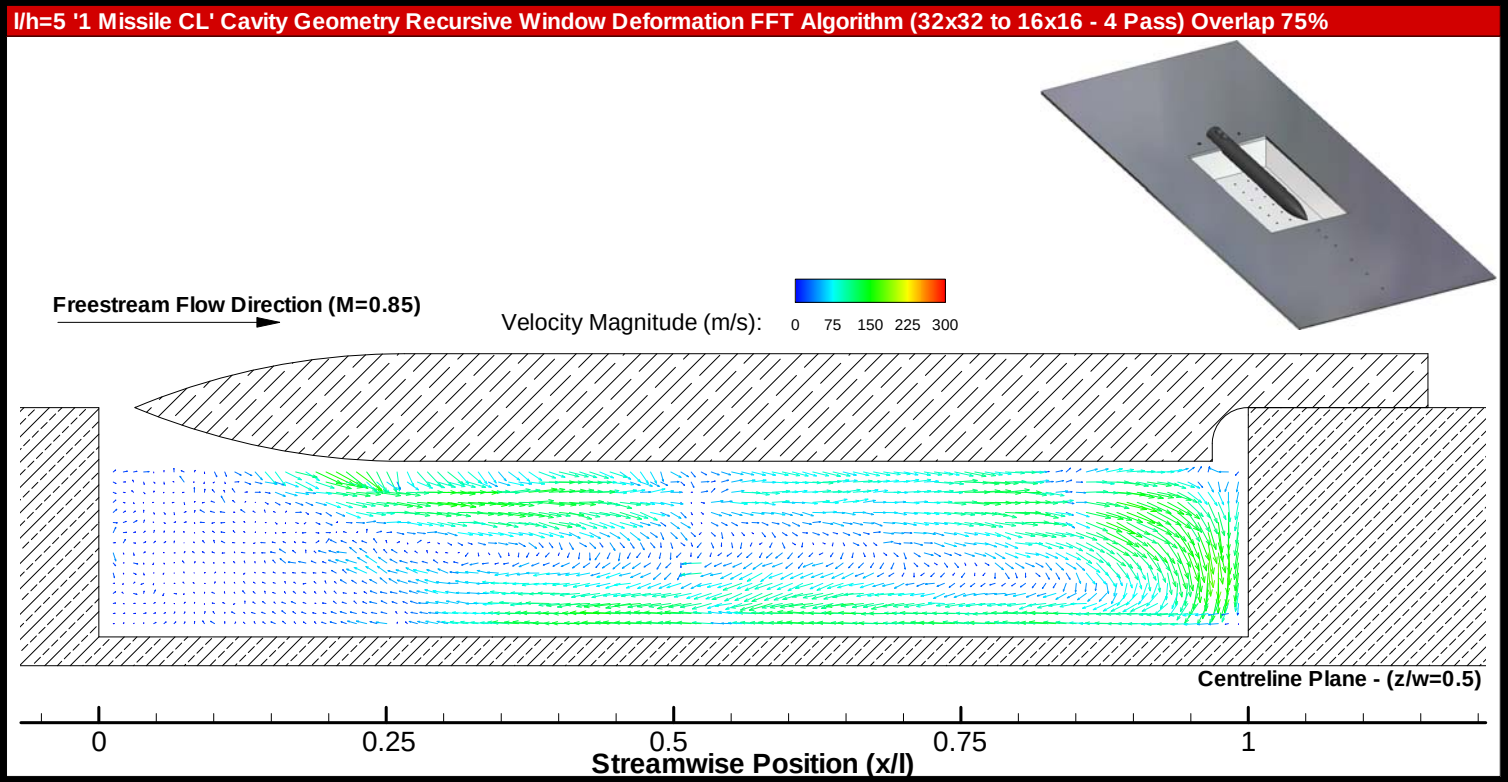

Centreline velocities – 3 missiles

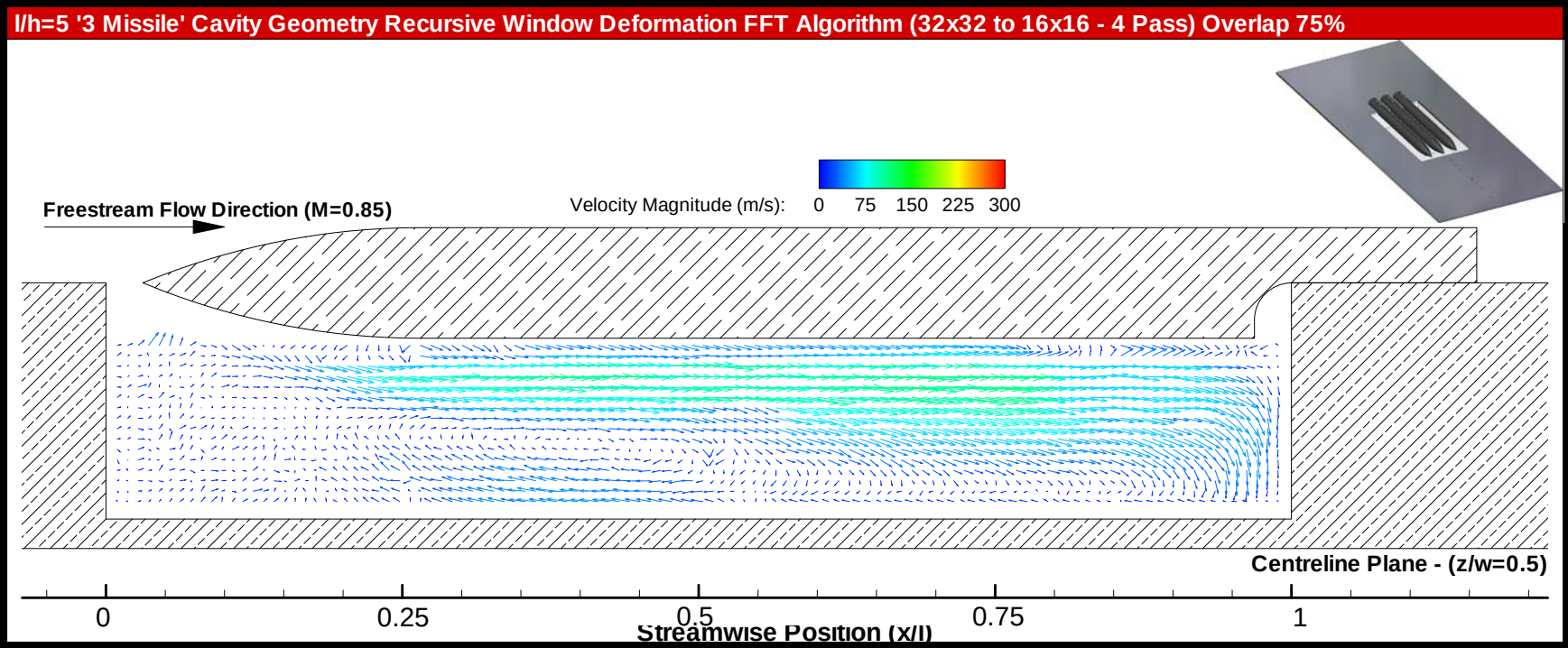

3D flowfield – l/h=14

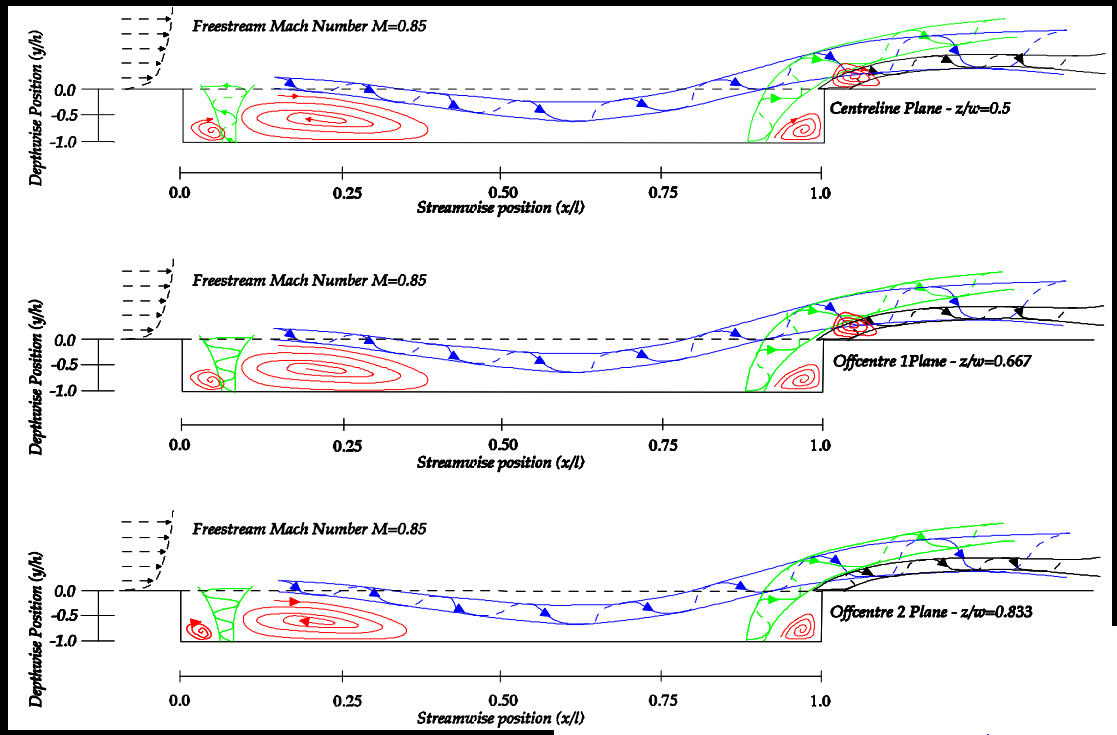

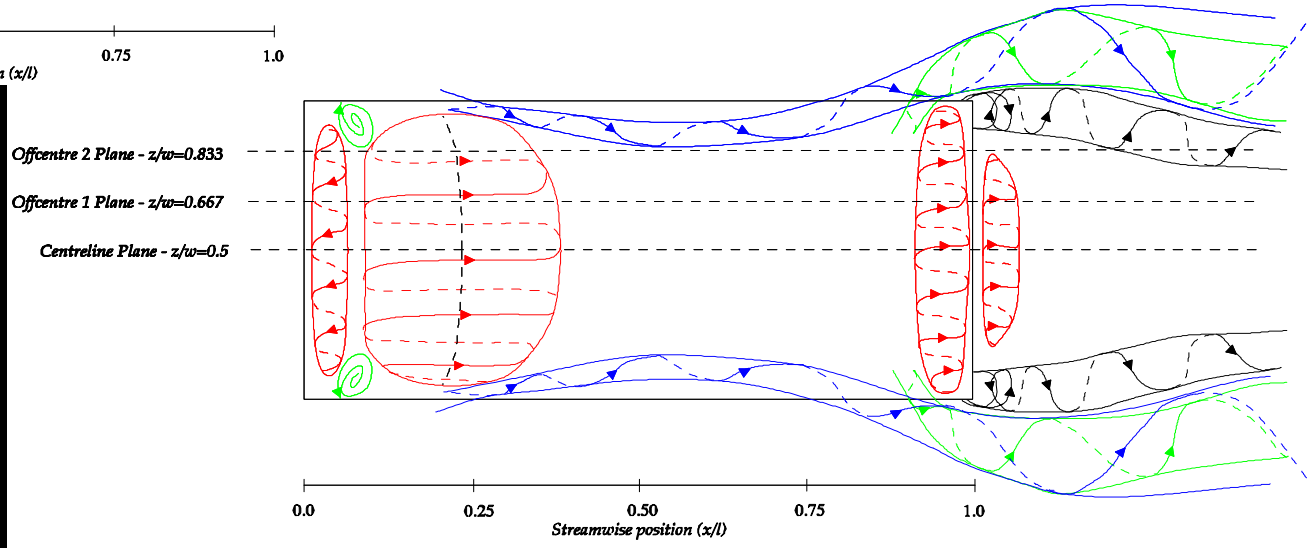

Knowles et al

DEFENCE ACADEMY OF THE UNITED KINGDOM
Cranfield UNIVERSITY
Defence College of Management and Technology

Conclusions

- An integrated experimental and computational study of 3D transonic cavity flows has been presented
- Cavity flow categorisation is seen to depend on boundary layer thickness as well as cavity length to depth ratio
- URANS CFD with the Realizable k-e model predicts a free shear layer which is too stiff

QUESTIONS?

Knowles et al

DEFENCE ACADEMY
OF THE UNITED KINGDOM
Cranfield UNIVERSITY
Defence College of Management and Technology